

The activation of *Chlamydomonas reinhardtii* alpha amylase 2 by glutamine requires its N-terminal aspartate kinase-chorismate mutase-tyrA (ACT) domain

Lisa Scholtysek¹  | Ansgar Poetsch^{2,3}  | Eckhard Hofmann⁴  |
Anja Hemschemeier¹ 

¹Faculty of Biology and Biotechnology, Photobiotechnology, Ruhr University Bochum, Bochum, Germany

²Faculty of Biology and Biotechnology, Department for Plant Biochemistry, Ruhr University Bochum, Bochum, Germany

³School of Basic Medical Sciences, Nanchang University, Nanchang, China

⁴Faculty of Biology and Biotechnology, Protein Crystallography, Ruhr University Bochum, Bochum, Germany

Correspondence

Anja Hemschemeier, Faculty of Biology and Biotechnology, Photobiotechnology, Ruhr University Bochum, Universitätsstr. 150, Bochum 44801, Germany.
Email: anja.hemschemeier@ruhr-uni-bochum.de

Funding information

This study was funded by the Deutsche Forschungsgemeinschaft (DFG; German Research Foundation) (RTG 2341: Microbial Substrate Conversion [MiCon]) and the German Federal Ministry of Education and Research, within the ERA-MIN2 framework, project MiCCuR (033RU011B).

Abstract

The coordination of assimilation pathways for all the elements that make up cellular components is a vital task for every organism. Integrating the assimilation and use of carbon (C) and nitrogen (N) is of particular importance because of the high cellular abundance of these elements. Starch is one of the most important storage polymers of photosynthetic organisms, and a complex regulatory network ensures that biosynthesis and degradation of starch are coordinated with photosynthetic activity and growth. Here, we analyzed three starch metabolism enzymes of *Chlamydomonas reinhardtii* that we captured by a cyclic guanosine monophosphate (cGMP) affinity chromatography approach, namely, soluble starch synthase STA3, starch-branching enzyme SBE1, and α -amylase AMA2. While none of the recombinant enzymes was directly affected by the presence of cGMP or other nucleotides, suggesting an indirect binding to cGMP, AMA2 activity was stimulated in the presence of L-glutamine (Gln). This activating effect required the enzyme's N-terminal aspartate kinase-chorismate mutase-tyrA domain. Gln is the first N assimilation product and not only a central compound for the biosynthesis of N-containing molecules but also a recognized signaling molecule for the N status. Our observation suggests that AMA2 might be a means to coordinate N and C metabolism at the enzymatic level, increasing the liberation of C skeletons from starch when high Gln levels signal an abundance of assimilated N.

KEYWORDS

ACT domain, alpha-amylase, cGMP, *Chlamydomonas*, glutamine, starch

1 | INTRODUCTION

Organisms need to acclimate to external or internal fluctuations in nutrient availability to adjust the biosynthesis of cell components that are mostly composed of more than one element. Carbon (C) and nitrogen (N) are the most abundant elements in cells, and their assimilation

and distribution are tightly regulated to maximize growth. Plants and algae acquire N mostly through the assimilation of nitrate, nitrite, or ammonium (Calatrava et al., 2023; Liu et al., 2022). Ammonium, the product of most N assimilation pathways, is ultimately transferred to L-glutamate (Glu) by glutamine synthetase (GS), forming L-glutamine (Gln). The Glu acceptor molecule is recycled by the transfer of the

This is an open access article under the terms of the [Creative Commons Attribution-NonCommercial](https://creativecommons.org/licenses/by-nc/4.0/) License, which permits use, distribution and reproduction in any medium, provided the original work is properly cited and is not used for commercial purposes.

© 2024 The Author(s). *Plant Direct* published by American Society of Plant Biologists and the Society for Experimental Biology and John Wiley & Sons Ltd.

amino group to α -ketoglutarate (α KG; or 2-oxoglutarate) by glutamate synthase (also termed glutamine oxoglutarate aminotransferase [GOGAT]), and the resulting net Glu is employed as an amino group donor for subsequent biosynthetic pathways.

In photosynthetic organisms, C is mostly acquired through carbon dioxide (CO_2) assimilation by the Calvin–Benson–Bassham (CBB) cycle. Triose phosphates and hexoses thus produced can be employed for anabolic processes directly or stored as starch, an insoluble glucose polymer, and one of the most important storage polymers in the Archaeplastida. Transitory starch is formed during the daily illumination period and degraded regularly, mostly in darkness, to provide C skeletons and energy for growth and maintenance, whereas storage starch serves as a mid- to long-term resource for periods of starvation, seedling development, or perennation. The importance of coordinating starch metabolism with growth and survival is reflected by multiple regulatory interventions in starch biosynthesis and degradation, many of which have been discovered rather recently (Abt & Zeeman, 2020; Geigenberger, 2011; Santelia et al., 2015).

Starch consists of two polyglucan subfractions, which are both α -1,4-linked glucose polymers branched through α -1,6 glycosidic bonds (Bertoft, 2017). The major subfraction is amylopectin, which is regularly branched and forms the semicrystalline backbone of starch. Amylose, the minor fraction, usually consists of shorter glucose chains and only few branches. The enzymatic steps of starch biosynthesis and degradation are quite well understood (Deschamps et al., 2023; Zeeman et al., 2010). The glucose substrate for starch biosynthesis derives from fructose-6-phosphate, an intermediate of the CBB cycle, by the actions of phosphoglucose isomerase and phosphoglucomutase. The first committed substrate for starch biosynthesis is adenosine diphosphate (ADP)-glucose, produced by ADP-glucose pyrophosphorylase (AGPase) from adenosine triphosphate (ATP) and glucose-1-phosphate. ADP-glucose is used by starch synthases to elongate glucan chains through α -1,4-glycosidic bonds, releasing ADP upon catalysis. Starch synthases belong to at least six different classes, soluble starch synthases SSI to SSV (although SSV is catalytically inactive) and granule-bound starch synthase, and enzymes belonging to different classes have distinct roles in starch biosynthesis (Abt & Zeeman, 2020; Deschamps et al., 2023; Irshad et al., 2021; Schwarte et al., 2013).

Branches are introduced into the polyglucan by starch-branching enzymes (SBEs) that cleave an α -1,4 glycosidic bond and form a new α -1,6 bond between the cleaved glucan and a glucose molecule of a linear chain. SBEs are grouped into class I and class II, and analyses of mutant plants and algae showed that the loss of class II branching enzymes usually results in notable phenotypes, whereas the absence of class I branching enzymes appears to have little or no consequences (Courseaux et al., 2023; Tetlow & Emes, 2014, and references therein). Two types of debranching enzymes—isoamylases and limit dextrinases (also termed pullulanases)—hydrolyze α -1,6 bonds (Deschamps et al., 2023; Zeeman et al., 2010). In the direction of starch granule formation, debranching enzymes “trim” the branches

of amylopectin so that the highly ordered structure of starch can be formed. Disproportionating enzymes or α -1,4 glucanotransferases transfer maltooligosaccharides from a donor to an acceptor glucan. In the unicellular green alga *Chlamydomonas reinhardtii* (*Chlamydomonas* henceforth), their role appears to be a “rescue” of glucan chains released upon trimming (Wattebled et al., 2003, and references therein), but in the Brassicacean model plant *Arabidopsis thaliana* (*Arabidopsis* henceforth), they seem to be involved in starch degradation (Critchley et al., 2001; Li et al., 2017). Likewise, starch phosphorylases that reversibly catalyze the phosphorolytic cleavage of α -1,4-glucosidic bonds in linear chains, releasing glucose-1-phosphate, appear to have roles both in starch biosynthesis and degradation (Pfister & Zeeman, 2016).

For degradation, the insoluble starch granule must be made accessible to hydrolytic enzymes (Stitt & Zeeman, 2012; Zeeman et al., 2010). This is achieved by the phosphorylation of glycosyl residues by α -glucan, water dikinases and phosphoglucan, water dikinases. Amylases, debranching enzymes, and starch phosphatases act in concert to hydrolyze the polyglucan chains: Beta-amylases are maltose-liberating exoamylases that require the phosphate groups at glucose moieties to be removed by starch phosphatases. Debranching enzymes remove branches that inhibit β -amylase activity. Alpha-amylases hydrolyze endogenous α -1,4-glycosidic bonds, and their importance for starch degradation appears to vary depending on the species. In *Arabidopsis*, β -amylases are the major starch hydrolyzing enzymes (Yu et al., 2005), whereas α -amylase I-1 is required for normal starch degradation in rice (Asatsuma et al., 2005). In *Chlamydomonas*, predominating α -amylase activity in partially purified amylase preparations was suggested (Levi & Gibbs, 1984). However, a *Chlamydomonas* mutant with a disruption of the β -amylase gene *AMB1* showed clear defects in storage starch degradation (Tunçay et al., 2013).

Starch synthesis and degradation are regulated on multiple levels that sometimes converge on one enzyme. For most catalytic steps, several enzyme isoforms are encoded by plant and algal genomes that differ in catalytic characteristics and/or domain architectures (Deschamps et al., 2023). The starch synthases of different classes, although in most cases sharing the catalytic domain, have diverse N-termini (Irshad et al., 2021; Qu et al., 2018; Schwarte et al., 2013), and the N-terminal coiled-coil domain of *Arabidopsis* SS4, for example, is required for correct localization and starch granule initiation (Lu et al., 2018; Raynaud et al., 2016). Differential gene expression also plays a role (e.g., Qu et al., 2018; Smith et al., 2004), but many regulatory signals work directly on the enzymes. Depending on plant species and localization, the first committed enzyme, AGPase, can be allosterically activated by 3-phosphoglycerate, the product of CO_2 fixation by ribulose-1,5-bisphosphate carboxylase/oxygenase, and inhibited by phosphate (Figueroa et al., 2022; Geigenberger, 2011). Starch phosphorylases of several species, including *Chlamydomonas*, are inhibited by ADP-glucose (Dauvillée et al., 2006; Hwang et al., 2010). A number of enzymes of the starch metabolism are regulated through reversible disulfide bond formation (Kötting et al., 2010; Santelia



et al., 2015; Skryhan et al., 2018). For example, AGPase activity and sensitivity to 3-phosphoglycerate are increased by the reduction of specific cysteine thiol groups, whereas the oxidative formation of a disulfide bond has the opposite effect (Figueroa et al., 2022; Geigenberger, 2011). Additional examples are the *Arabidopsis* β -amylase BAM1 (Sparla et al., 2006; Valerio et al., 2011) and α -amylase AMY3 (Seung et al., 2013) or potato α -glucan water dikinase (Mikkelsen et al., 2005) that are active in their reduced, but hardly active in their oxidized form.

Starch metabolism enzymes are also modified by protein phosphorylation (Kötting et al., 2010), which affects protein activity, for example, in the case of wheat SBElIa and SBElIb, as well as protein complex formation (Mehrpuoyan et al., 2021; Tetlow et al., 2004). Indeed, enzymes of the starch metabolism have been detected in (multi)protein complexes, suggesting a concerted action of these enzymes or regulatory interactions (Geigenberger, 2011; Kötting et al., 2010). In some cases, protein complexes are formed between catalytically active enzymes and inactive isoforms or with dedicated scaffolding or targeting proteins (Abt & Zeeman, 2020). One example is *Arabidopsis* LIKE SEX4 1, an inactive starch phosphatase that interacts with plastidial β -amylases and is required for normal starch degradation (Schreier et al., 2019).

Previously, we showed that the *Chlamydomonas* nitric oxide (NO)-sensitive guanylate cyclase CYG12, which we had suspected to be involved in hypoxic acclimation, apparently plays pleiotropic roles (Düner et al., 2018): An algal strain in which the CYG12 transcript was post-transcriptionally downregulated by a micro-RNA approach showed impaired growth in hypoxia and darkness and additionally photosynthetic defects in aerobiosis in the light. The strain also exhibited aberrant patterns of consuming acetate from the medium and degrading internal starch reserves. Here, we show the results of an affinity chromatography approach that aimed to capture proteins that bind to cyclic guanosine monophosphate (cGMP), the product of guanylate cyclase activity. With this technique, we aimed to identify possible targets of CYG12 signaling. We were surprised that, besides identifying several proteins predicted to bind cyclic nucleotide monophosphates (cNMPs), we found 15 proteins that are involved in the metabolism of starch. We selected three enzymes for biochemical analyses: soluble starch synthase 3 (STA3 or SSS3A), SBE1, and α -amylase 2 (AMA2). We focused on AMA2, because this protein has an N-terminal aspartate (Asp) kinase-chorismate mutase-TyrA (ACT) domain, known to bind small ligands and thereupon regulating enzymatic activity (Grant, 2006; Lang et al., 2014). Notably, while none of the three selected enzymes was directly affected by cGMP or additional nucleotides *in vitro*, suggesting that they might bind to cGMP indirectly, we observed that AMA2 activity was increased in the presence of Gln. This effect required the presence of the ACT domain and could be diminished by selected amino acid exchanges. This result suggests that within the cell, AMA2 might be important for the coordination of N and C metabolism, being stimulated to release C skeletons when N is sufficiently available as indicated by its first assimilation product, Gln.

2 | MATERIALS AND METHODS

2.1 | cGMP interaction chromatography and protein identification

2.1.1 | Preparation of *Chlamydomonas* soluble protein extracts

Soluble proteins were obtained from *Chlamydomonas* wild-type strain CC-124 mt⁻ [137c] (*Chlamydomonas* Resource Center, University of Minnesota, MN, USA). Cells were grown in liquid Tris acetate phosphate (TAP) medium (Harris, 1989) at 20°C upon continuous bottom-up illumination of 100 μ mol of photons \times m⁻² \times s⁻¹ (two Osram Lumilux Cool White light bulbs alternating with one Osram Fluora bulb) on a reciprocal shaker set to 100 rpm. At a density of 3×10^6 cells \times mL⁻¹, the cells were harvested by centrifugation (10 min, 3200 g, 4°C). One gram of fresh weight was resuspended in 2 mL of extraction buffer (50 mM Tris-HCl, pH 7.4, .25 M sucrose, 1 mM EDTA, .1 mM MgSO₄, 10 mM KCl, 5 mM ascorbic acid, 1 mM phenylmethylsulfonyl fluoride, 1 \times protease inhibitor cocktail [cComplete ULTRA tablets, EDTA-free, Roche], .5% (w/v) polyvinylpyrrolidone). Cell lysis was done by sonication on ice (Branson Sonifier 250; output 40%, 6 \times 30 s with 90 s breaks). The lysate was centrifuged (30 min, 16,000 g, 4°C), and the supernatant was filtered through a .2 μ m syringe filter (cat-no. 83.1826.001; Sarstedt, www.sarstedt.com). The protein concentration of the filtered lysate was determined using the Bio-Rad Protein Assay Dye Reagent Concentrate (Bio-Rad; www.bio-rad.com) and bovine serum albumin (BSA) as standard and was subsequently adjusted to a concentration of 3 mg \times mL⁻¹ with extraction buffer.

2.1.2 | cGMP interaction chromatography

cGMP interaction chromatography was done based on a protocol from Donaldson and Meier (2013) and Donaldson et al. (2016). All steps were performed in the cold room at 8°C. Two types of cGMP-functionalized agarose beads from the Biolog Life Science Institute (www.biolog.de) (2'-AHC-cGMP-agarose [2'-O-(6-aminohexylcarbamoyl)guanosine-3', 5'-cyclic monophosphate-agarose; cat-no. A 059] and 2-AH-cGMP-agarose [N²-(6-aminohexyl)guanosine-3', 5'-cyclic monophosphate-agarose; cat-no. A 056]) as well as a control bead material functionalized with ethanolamine (EtOH-NH-agarose; cat-no. E 010) were prepared by mixing 200 μ L of resuspended bead material with 1 mL of assay buffer (extraction buffer without polyvinylpyrrolidone) and incubating the mixture for 2 h on a shaker at 300 rpm. Afterward, the agarose beads were harvested by mild centrifugation (30 s, 100 g), and the supernatants were carefully removed. Each bead type was mixed with 1 mL of *Chlamydomonas* protein extract and incubated overnight under continuous shaking at 300 rpm. Following this incubation, the agarose beads were harvested by gentle centrifugation (30 s, 50 g), and the supernatant was removed. The beads were then resuspended in 1 mL of assay buffer, incubated for 5 min mixing at 300 rpm, and harvested

by centrifugation. After discarding the supernatant, this washing step was repeated five times. Afterward, nucleotides dissolved in assay buffer were employed to elute proteins with different nucleotide-binding characteristics, namely, in this order, 100 mM ADP, 100 mM guanosine monophosphate (GMP), 10 mM cyclic adenosine monophosphate (cAMP), 25 mM cAMP, 10 mM cGMP, and 100 mM cGMP. In each case, the agarose beads were resuspended in 200 μ L of these solutions and incubated for 5 min at 300 rpm. After centrifugation, the supernatants were collected for subsequent protein identification. Each elution step was followed by a washing step as described above.

2.1.3 | Preparation of tryptic peptides

For protein identification by mass spectrometry, the six elution fractions of each bead type were prepared for in-gel tryptic digest. First, proteins were precipitated by mixing each sample with 800 μ L of -20°C cold acetone. After incubation overnight at -20°C , the samples were centrifuged (10 min, 14,000 g, 4°C), the supernatant was discarded, and the protein pellets were briefly dried in a sterile bench. Then, the protein pellets were resuspended in 15 μ L ultrapure water and 4 μ L sodium dodecyl sulfate polyacrylamide gel electrophoresis (SDS-PAGE) sample buffer (.05 M Tris-HCl pH 8, 5% (v/v) glycerol; 1.5% (w/v) SDS; .05 mg \times mL $^{-1}$ bromophenol blue; 2.5% (v/v) β -mercaptoethanol), incubated at 95°C for 5 min, and loaded on 15% SDS polyacrylamide gels, separated by empty lanes. The agarose beads remaining after the final washing step were directly dissolved in SDS-PAGE sample buffer, heated, and loaded onto the gels. After the samples had run into the separating gel, electrophoresis was stopped, the gels were stained with Coomassie, and the protein containing parts were excised. The gel pieces were destained by first incubating them in 200 μ L of 50 mM ammonium bicarbonate (ABC) for 20 min and mixing at 300 rpm, followed by several incubation steps in 25 mM ABC and 50% (v/v) acetonitrile (ACN), until the gel pieces were colorless. The gel pieces were dehydrated in 100% (v/v) ACN and then rehydrated with 30 μ L of 3.33 μ g \times mL $^{-1}$ trypsin (cat-no. T6567 from Sigma-Aldrich/Merck, www.sigmaaldrich.com) in 25 mM ABC. Afterward, 25 mM ABC was added to fully cover the gel pieces, and tryptic digest was performed at 37°C overnight upon mixing at 300 rpm. After transferring the supernatant to a fresh reaction tube, 70 μ L of 50% (v/v) ACN and 1% (v/v) formic acid (FA) were added to the gel pieces, followed by an incubation at room temperature and mixing at 300 rpm for 20 min. After centrifugation at 14,000 g and 4°C for 1 min, the supernatant was combined with the first supernatant. This latter extraction step was repeated once. After the addition of 30 μ L of 305 mM ammonium carbonate and .7 mM EDTA, the samples were completely dried in a vacuum concentrator at room temperature. The pellets were frozen at -20°C until further use.

2.1.4 | Mass spectrometric analyses

According to Cormann et al. (2016), the peptide pellets were resuspended in 20 μ L of .1 (v/v) % FA, injected into a UPLC Symmetry C₁₈

trapping column (5 μ m, 180 μ m \times 20 mm), and afterward transferred to a UPLC BEH C₁₈ column (1.7 μ m, 75 μ m \times 150 mm) using a nanoACQUITY UPLC system (all from Waters, www.waters.com). The temperature of the column oven was set to 45°C . Elution of peptides was achieved with a multistep gradient of buffer A (.1% (v/v) FA) to buffer B (.1% FA in ACN) at a flow rate of .4 μ L \times min $^{-1}$ (0–5 min: 1% buffer B; 5–10 min: 5% buffer B; 10–175 min: 40% buffer B; 175–200 min: 99% buffer B; 200–210 min: 1% buffer B). Coupling to the mass spectrometer (Orbitrap Elite; Thermo Fisher Scientific, www.thermofisher.com) was achieved via a PicoTip Emitter (SilicaTip, 30 μ m; New Objective, www.newobjective.com), and the spray voltage was at 1.5–1.8 kV. The temperature of the desolvation capillary was set to 200°C . Linear ion trap and Orbitrap were run in parallel during a full scan between 300 and 2000 m/z and a resolution of 240,000 on the orbitrap. MS/MS spectra of the 20 most intense precursors were detected in the ion trap. For collision-induced dissociation, relative collision energy was set to 35%, and dynamic exclusion was enabled (repeat count of one; 1 min exclusion duration window). Ions with an unassigned charge or singly or doubly charged ions were rejected.

The cGMP affinity chromatography experiment was done in two independent experiments, and computational protein identification was done on both sample sets simultaneously. The MaxQuant software (version 1.6.7.0) was used for data analysis, with all false discovery rates set to .01. Minimum peptide length was set to 6; maximal missed cleavages were set to 2; and methionine oxidation and N-terminal acetylation were included as possible modifications. Decoy mode (revert) was enabled, and common protein contaminants were included. Protein identification was done against *C. reinhardtii* v5.6 proteins (Creinhardtii_281_v5.6.protein) to which the chloroplast proteome (derived from sequence FJ423446.1 at the European Nucleotide Archive; www.ebi.ac.uk/ena/) and mitochondrial protein sequences (from GenBank NC_001638) had been added manually.

2.2 | Heterologous production and purification of *Chlamydomonas* starch metabolism enzymes and variants

2.2.1 | Generation of expression plasmids

The *Chlamydomonas* coding sequences for AMA2 (α -amylase; Cre08.g362450.t1.2; note that all gene identifiers refer to the *Chlamydomonas* genome version v5.6 at Phytozome 13), SBE1 (SBE; Cre06.g289850.t1.1), and STA3 (Cre06.g282000.t2.1) were cloned into the *Escherichia coli* expression vector pASK-IBA7 (IBA Lifesciences GmbH; www.iba-lifesciences.com/). Expression from this vector equips the target protein with an N-terminal *Strep*-tactin affinity tag (*Strep*-tag II), followed by a factor Xa cleavage site (Figure S1). Oligonucleotides were designed using the Primer D'Singer 1.1 software (IBA Lifesciences GmbH) to amplify the coding sequences including the putative chloroplast targeting peptides (Table 1). In the case of AMA2, protein variant Δ AMA2 was additionally generated. It consists of the

TABLE 1 Oligonucleotides employed for amplifying the coding sequences of the selected enzymes.

Target protein	Oligonucleotides employed for amplifying coding sequences for subsequent cloning into pASK-IBA7
STA3	F: 5'-ATGGTAGGTCTCAGCGCGCTCGTCTATGGGACGGGC-3' R: 5'-ATGGTAGGTCTCATATCACGCCTTCAGCGCTGAGAAGTAG-3'
SBE1	F: 5'-ATGGTAGGTCTCAGCGCGCTGCGAGCCGCTTCAGGG-3' R: 5'-ATGGTAGGTCTCATATCACACCACTTCGTCGCCGCTGC-3'
AMA2	F: 5'-ATGGTAGGTCTCAGCGCGACAGGTCGCTTCTCTCCAGG-3' R: 5'-ATGGTAGGTCTCATATCAGTGTGGCCCTCCACACGG-3'
ΔAMA2	F: 5'-ATGGTAGGTCTCAGCGCCTGGCCACCGAGCCGGAGAA-3' R: 5'-ATGGTAGGTCTCATATCAGTGTGGCCCTCCACACGG-3'

Note: Oligonucleotides employed for amplifying the sequences coding for STA3 (Cre06.g282000.t2.1), SBE1 (Cre06.g289850.t1.1), and AMA2 (Cre08.g362450.t1.2) as well as AMA2 without the predicted aspartate kinase-chorismate mutase-tyrA domain (ΔAMA2). *Bsa*I restriction sites (5'-GGTCTC(N₁)/(N₅)-3'), used for cloning into the expression vector pASK-IBA7, are underlined.

Abbreviations: F, forward, R, reverse.

predicted amylase domain only and lacks the N-terminal 269 amino acids encompassing the putative chloroplast transit peptide and the predicted ACT domain as well as the sequence following the ACT domain up to the predicted amylase domain (Figure S1). All sequences were amplified from total cDNA obtained from *Chlamydomonas* strain CC-124 mt⁻ as described in Huwald et al. (2015). Polymerase chain reactions (PCRs) were done employing the KAPA HiFi HotStart ReadyMix PCR Kit (#KK2601; Roche Sequencing, <https://sequencing.roche.com/en.html>). Sequences and vector were cut by *Bsa*I followed by ligation and transfection into *E. coli* DH5α by heat shock transformation. The cells were selected on LB agar plates (LB Lennox; Carl Roth GmbH, www.carlroth.com) containing 100 μg × mL⁻¹ ampicillin, and colonies were subsequently grown in liquid LB Broth (Lennox) medium with 100 μg × mL⁻¹ ampicillin. Plasmid isolation was done employing the GeneJet™ Miniprep kit (ThermoFisher Scientific), and sequencing was performed by the DNA sequencing service at the chair for biochemistry, Biochemistry I, receptor biochemistry, at Ruhr University Bochum, Germany.

2.2.2 | Generation of AMA2 amino acid exchange variants

Single amino acids in the predicted ACT domain of AMA2 were exchanged by site-directed mutagenesis of the AMA2 coding sequence within the pASK-IBA7 vector employing QuikChange PCR. Mismatched oligonucleotides were designed according to Zheng et al. (2004) and are listed in Table 2. Amplified PCR products were digested with *Dpn*I and afterward transfected into *E. coli* DH5α by heat shock transformation. Plasmid isolation and sequencing were done as described above.

2.2.3 | Heterologous protein production

For heterologous protein production, the expression vectors were introduced into *E. coli* Rosetta™ (DE3) by electroporation. Precultures

TABLE 2 Oligonucleotides employed for generating AMA2 amino acid exchange variants.

AMA2 variant	Oligonucleotides employed for introducing mutations into the AMA2 sequence
D106F	F: 5'-GGCAAGTTTAAAGGCGCACCTGCTG-3' R: 5'-GCCTTAAACTTGCCCTCTACCGTCAC-3'
L110G	F: 5'-GCACGGCCTGATGAGCCTGAC-3' R: 5'-CATCAGGCCGTGCGCCTTGTC-3'
G122D	F: 5'-GCGCCGATCTGACCGTCATCTC-3' R: 5'-GTCAGATCGGCGCTGGAGAAG-3'
G135D	F: 5'-GACGACGATCGCGTGTGGATG-3' R: 5'-GCACGCGATCGTCTACTG-3'
F141G	F: 5'-GGATGTCGGCCGCGTGCAGACC-3' R: 5'-CACGCGCCGACATCCAGCAGC-3'
G148D	F: 5'-CGCTGATGATAAGAAGGTGCC-3' R: 5'-CCTTCTTATCATCAGCGGTCTGC-3'

Note: The codons that introduce mutations in the AMA2 coding sequence are underlined. The numbers in column "AMA2 variant" refer to the exchanged amino acid of the native protein including the N-terminal methionine residue.

Abbreviations: F, forward, R, reverse.

were grown in 100 mL of LB medium containing 100 μg × mL⁻¹ ampicillin and 25 μg × mL⁻¹ chloramphenicol over night at 37°C, shaking at 120 rpm. Expression cultures were then inoculated to an OD₆₀₀ of .05 in 500 mL Terrific-Broth medium (12 g × L⁻¹ tryptone, 24 g × L⁻¹ yeast extract, .5% (v/v) glycerol, 17 mM KH₂PO₄, 72 mM K₂HPO₄) supplemented with 2 mM MgCl₂, 100 μg × mL⁻¹ ampicillin, and 10 μg × mL⁻¹ chloramphenicol in 2 L Erlenmeyer flasks. These cultures were incubated at 37°C, shaking at 120 rpm, until they had reached an OD₆₀₀ between .5 and .6 (expression of STA3 and SBE1) or between .9 and 1 (expression of AMA2). Expression of the constructs was then induced by the addition of .2 μg × mL⁻¹ anhydrotetracycline from a stock solution of 2 mg × mL⁻¹ in dimethyl sulfoxide, and the cultures were incubated overnight at 21°C, shaking at 120 rpm on a rotary shaker.

2.2.4 | Protein purification

After about 17 h of expression, the *E. coli* cells were harvested by centrifugation for 20 min at 4430 g at 4°C. The cell pellet was resuspended in buffer W (100 mM Tris-HCl pH 8, 150 mM NaCl, .1 mM EDTA). Cell lysis was done by sonication on ice (output 50%, four cycles of 45 s, 1 min breaks) with a Branson Sonifier 250 (Branson; www.emerson.com/en-us/automation/branson). The lysate was centrifuged at 180,000 g for 1 h at 4°C, and the supernatant was subsequently passed through a sterile filter (.2 μm pore diameter). The cleared lysate was loaded onto a gravity-flow column with Strep-Tactin® Superflow® high-capacity resin (IBA Lifesciences GmbH) pre-equilibrated with buffer W. Washing was done with 20 mL buffer W and elution by applying 10 mL buffer E (buffer W with 2.5 mM desthiobiotin). Elution fractions were pooled, and proteins were concentrated using a 30 kDa Amicon Ultra-4 Centrifugal Filter Unit (Merck Milipore; www.merckmillipore.com). Protein concentration was determined employing the Bio-Rad Protein Assay Dye Reagent Concentrate (Bio-Rad) using BSA as standard. Size and purity of the proteins were routinely checked by separating protein solutions through SDS-PAGE.

2.2.5 | Size exclusion chromatography (SEC)

SEC was performed to determine the oligomeric state of AMA2 and was done using ÄKTA protein purification systems and a Superdex 200 Increase 10/300 GL column (24 mL column volume). Buffer W was used for equilibration and elution. The flow rate was set to .75 mL × min⁻¹, and proteins were loaded through a sample loop. Calibration of the column was performed using the Gel Filtration Markers Kit for Protein Molecular Weights 12,000–200,000 Da (#MWGF200; Sigma-Aldrich/Merck, www.sigmaldrich.com).

2.3 | In vitro activity assays

2.3.1 | Alpha-amylase assay

α-amylase activity was analyzed by recording the absorption of starch-iodine complexes adapted from the method of Xiao et al. (2006). Enzyme concentrations, buffers, and starch types differed depending on the aim of the assay. In all cases, enzymes diluted in 200 μL of buffer were mixed with 200 μL of .7 mg × mL⁻¹ starch dissolved in ultrapure water and then incubated shaking at 300 rpm for 30 min at 30°C except for experiments aimed to determine temperature optima. The reaction was stopped by adding 100 μL of 1 M HCl. The solutions were then mixed with 500 μL of iodine solution (.52 mg × mL⁻¹ I₂ and 5.2 mg × mL⁻¹ KI), and the absorption was determined at λ = 580 nm against 500 μL of buffer mixed with 500 μL of iodine solution. A control sample was prepared for each assay in the same way but without enzymes. Starch calibration curves were generated using 20 to 200 μg starch. Enzyme activity (U) was

defined as the decrease of 1 mg of iodine-stainable starch per minute. Specific activity was calculated according to the formula $U \times \mu\text{mol}^{-1} = (A580_{\text{control}} - A580_{\text{sample}}) / ((A580 \times \text{mg starch}^{-1}) \times 30 \text{ min} \times \mu\text{mol enzyme})$. Routinely, soluble potato starch was employed as substrate (cat.-no. S2630 from Sigma-Aldrich/Merck). However, we also tested enzyme activities on *Chlamydomonas* storage starch (see the procedure to isolate native starch below).

Three different buffers were employed depending on the purpose; the buffer type is always indicated in the text. Routine assays to check for the activities of freshly prepared enzyme batches were performed in .1 M potassium phosphate buffer, pH 7. In several cases, we used a buffer designed to approach standard cellular ion concentrations, which we termed “physiological buffer” (50 mM potassium phosphate, pH 7.4, 50 mM KCl, 10 mM NaCl, .5 mM MgCl₂, 100 nM CaCl₂). For determining pH optima, .1 M Britton–Robinson buffer, pH 5.0 to 11.0 (boric acid, phosphoric acid, and acetic acid, titrated with sodium hydroxide to the desired pH), was employed (Britton & Robinson, 1931). Temperature optima were determined in Britton–Robinson buffer, pH 7.5, at incubation temperatures between 10°C and 50°C.

2.3.2 | SBE assay

The presence of SBE alters the absorption of the starch-iodine complex (e.g., Courseaux et al., 2023; Rammesmayr & Praznik, 1992), so that SBE1 activity was determined as described for α-amylase above. In addition to starch as substrate, SBE1 activity was determined in the presence of amylopectin (amylopectin from maize; cat.-no. 10120 from Sigma-Aldrich/Merck), which SBEs also employ as a substrate (e.g., Courseaux et al., 2023; Guan & Preiss, 1993). The assay was performed as described above, except that 200 μL of .9 mg × mL⁻¹ amylopectin dissolved in ultrapure water were added. In this case, absorption was measured at λ = 550 nm. pH and temperature optima were determined as described for α-amylase, except that .1 M Britton–Robinson buffer, pH 7, was used for the latter.

2.3.3 | Soluble starch synthase assay

Starch synthase activity was analyzed according to Kulichikhin et al. (2016) who established an assay in which ADP, released from ADP-glucose by starch synthase activity, is converted to NADPH by subsequent enzymatic reactions. First, STA3 dissolved in 200 μL water was added to a reaction mixture containing 50 mM HEPES-NaOH, pH 7.5, 1.4 mg amylopectin, and 15 mM dithiothreitol (DTT) in a total volume of 423 μL. A reference tube was prepared in the same way. The mixtures were preincubated for 2 min at 30°C before adding 27 μL of 20 mM ADP-glucose. The reference tube was immediately incubated at 100°C for 1 min to stop the reaction, while the reaction tube was incubated for 20 min at 30°C before stopping the reaction at 100°C. For all subsequent steps, reference and experimental tubes were processed in parallel. After allowing the reaction mixtures to cool down



to room temperature, the samples were centrifuged for 10 min at 10,000 g. Three hundred microliters of the supernatants were transferred to fresh tubes, and 200 μ L of solution 1 (50 mM HEPES-NaOH, pH 7.5, 200 mM KCl, 10 mM $MgCl_2$; 4 mM phosphoenolpyruvate) as well as 1.2 U pyruvate kinase (P1506; Sigma-Aldrich/Merck) were added to convert ADP and phosphoenolpyruvate to ATP and pyruvate. The reaction mixtures were incubated for 20 min at 30°C, and the reactions were stopped by incubation at 100°C for 1 min followed by centrifugation. The mixtures were then transferred to new tubes containing 400 μ L of solution 2 (50 mM HEPES-NaOH, pH 7.5, 10 mM glucose, 20 mM $MgCl_2$, 2 mM $NADP^+$), and the reaction was started by adding 1.4 U hexokinase (H5000; Sigma-Aldrich/Merck) and .36 U glucose-6-phosphate dehydrogenase (G7877; Sigma-Aldrich/Merck) to each tube. During this reaction, hexokinase employs ATP to form glucose-6-phosphate, which is oxidized by glucose-6-phosphate dehydrogenase, forming NADPH. The mixtures were incubated for 10 min at 30°C before the absorption of the reaction mixture was monitored at 340 nm against the reference mixture. The final absorbance value was recorded after 10 min. Enzyme activity (U) of soluble starch synthase was defined as the release of 1 μ mol of ADP, which is equivalent to the production of 1 μ mol of NADPH, per 1 min. The final amount of NADPH was calculated employing its specific absorption coefficient at $\lambda = 340$ nm ($6.22 \text{ L} \times \text{mmol}^{-1} \times \text{cm}^{-1}$) and related to the STA3 amount employed, taking into account all dilution steps. The pH optimum of STA3 was determined by replacing HEPES by Britton–Robinson buffer, pH 5 to 12, in the first reaction mixture. Controls were performed when necessary to test for any effects on the additional enzymes present in this assay. In these cases, STA3 was excluded and 100 μ M of ADP was added as substrate, whereas all other components and proceedings were the same as described above.

2.3.4 | Effect of small molecules on enzyme activities

To test for any influence of small molecules on enzyme activities, assays were conducted as described above, employing our “physiological buffer.” The additional molecules were added in concentrations indicated in Section 3. Proteinogenic amino acids, α KG, cGMP and cAMP, and GMP and adenosine monophosphate (AMP) were obtained from Sigma-Aldrich/Merck (www.sigmaaldrich.de). Cyclic diguanosine monophosphate (c-di-GMP) and guanosine-3',5'-bisdiphosphate (ppGpp) were obtained from Biolog Life Science Institute (C057; www.biolog.de/) and Jena Bioscience (NU-884; www.jenabioscience.com/), respectively.

2.3.5 | Effect of redox agents

To test the effects of reductants and oxidants, recombinant proteins were diluted to a concentration of 1 $\text{mg} \times \text{mL}^{-1}$ in 20 μ L of “physiological buffer.” After the addition of 5 mM of DTT or .1, 1, or 5 mM of

diamide, the reaction mixtures were incubated for 20 min at 23°C. As a control, the same protein dilutions were incubated in parallel without the addition of redox reagents. Afterward, in vitro activity assays were done as described above. Note that the first reaction mixture of the soluble starch synthase assay as described by Kulichikhin et al. (2016) routinely contains DTT, which was omitted for testing the effects of DTT and diamide on STA3.

2.4 | Purification of starch from *Chlamydomonas*

Native starch was purified from nitrogen (N)-limited *Chlamydomonas* cultures by a protocol modified from Delrue et al. (1992). *Chlamydomonas* strain CC-124 was first grown in liquid TAP medium as described above. To induce N deficiency, the cells were inoculated at a density of 3×10^6 cells $\times \text{mL}^{-1}$ in 250 mL of a modified TAP medium without any N source. After 5 days of growth, cells were harvested by centrifugation (6000 g for 20 min at 4°C), the pellet was washed in 100 mL 20 mM HEPES-KOH, pH 7.5, and the cell suspension was transferred to 50 mL conical centrifugation tubes. After an additional centrifugation step, the cell pellet was resuspended in 2 mL of ice cold 20 mM HEPES-KOH, pH 7.5, and this suspension was diluted with 10 mL of lysis buffer (300 mM sorbitol, 50 mM HEPES-KOH, pH 7.5, 2 mM EDTA, 1 mM $MgCl_2$, 1% (w/v) BSA). The algal cells were ruptured by sonication on ice (output 50%, six cycles of 30 s, 1 min breaks), and then, the lysate was distributed to 2 mL reaction tubes and centrifuged at 760 g for 10 min at 4°C. The supernatants were discarded, and the crude starch pellets were resuspended in 2 mL of lysis buffer. The suspensions were combined and carefully applied on a 24 mL Percoll gradient composed of three layers of 20%, 45%, and 60% Percoll in .9 \times lysis buffer. After centrifugation (15 min, 5900 g, 4°C), the purified starch pellet was rinsed with 1 mL of lysis buffer and centrifuged at 2000 g for 10 min at 4°C. The starch pellet was snap-frozen in liquid nitrogen and stored at -20°C . For in vitro enzyme assays, the starch pellet was thawed on ice and resuspended in 10 to 15 mL of distilled water. Starch concentration was analyzed by the starch–iodine method in different dilutions of the starch suspension, utilizing commercial soluble potato starch as a standard.

2.5 | In silico structure prediction and sequence analyses

The structure of an AMA2 dimer was predicted employing AlphaFold2-multimer as implemented in LocalColabfold (Evans et al., 2022; Jumper et al., 2021; Mirdita et al., 2022). Template information was applied, and no amber relaxation was used.

To generate alignments, we first extracted the AMA2 ACT domain sequence based on the AlphaFold2 models (also see Section 3). Residues 86 to 168 of the protein sequence Cre08.g362450.t1.2 were used as query in NCBI's Basic Local Alignment Search Tool BlastP against the nonredundant protein sequences database. The hits thus retrieved were manually inspected to reduce the

number of sequences. For example, many sequences from metagenomic annotations were omitted. Selected full-length sequences were analyzed by NCBI's Conserved Domains or InterPro (Paysan-Lafosse et al., 2023) predictions to identify additional domains (Table S1). The aligned sequences as provided by the original NCBI BlastP analysis of the selected proteins were combined, and a few sequences were manually added. These were the two ACT domains of *E. coli* GlnD (UniProt B6HZE1) (Zhang et al., 2010), the two ACT domains of *A. thaliana* ACR11 (Sung et al., 2011), and the putative ACT domain of *Chlamydomonas* STA4 (Cre12.g552200.t1.2). In these three latter cases, the AlphaFold models deposited in the AlphaFold Protein Structure Database (<https://alphafold.ebi.ac.uk/>; GlnD: B6HZE1, ACR11: Q9FZ47, STA4: A8IYK1) were inspected to extract the residues encompassing the ACT domain. The final list of sequences was subsequently aligned using Clustal Omega (Sievers et al., 2011).

2.6 | Accession numbers

Chlamydomonas sequence data from this article can be found in the *C. reinhardtii* v5.6 genome annotation at Phytozome 13 (https://phytozome-next.jgi.doe.gov/info/Creinhardtii_v5_6) under the accession numbers indicated in the text and in Data S1.

2.7 | Supplemental data files

Supporting information and Data S1 are available online.

3 | RESULTS

3.1 | cGMP affinity chromatography captured starch metabolism enzymes

We employed cGMP affinity chromatography to identify downstream effectors of *Chlamydomonas* guanylate cyclases. This method has been applied for animal cNMP-binding proteins (Kim & Park, 2003; Scholten et al., 2006) and adapted to *Arabidopsis* protein extracts (Donaldson & Meier, 2013). The procedure aims to enrich cGMP-binding proteins on agarose beads functionalized with cGMP, and sequential elution with ADP, GMP, and cAMP reduces the number of unspecific proteins (Scholten et al., 2006). A control with agarose beads functionalized with ethanolamine helps to eliminate proteins that bind to the agarose matrix. The procedure employs nondenatured proteins, so that it captures proteins that bind directly but also proteins that form complexes with proteins retained in the beads (Scholten et al., 2006, 2007).

We conducted the cGMP affinity chromatography experiment twice in independent experiments, using independent *Chlamydomonas* protein extracts. Only proteins for which at least two unique peptides were detected in any given elution or agarose bead fraction were regarded as truly being present. In total, 1246 *Chlamydomonas*

proteins were detected (Data S1, Sheet 1). Of these, 319 proteins were present with maximally one unique peptide and were therefore not considered further. Of the remaining 927 proteins (Data S1, Sheet 2), we considered a protein as present in an elution fraction or retained in one of the bead types when they were represented by at least two unique peptides in both replicates. In the case of the control bead fractions, however, we also had a look at proteins present only in one replicate to gain an idea about what types of proteins might be enriched by the bead material. One hundred eighty-three proteins were present with at least two unique peptides in both and 223 in either of the control replicates (Data S1, Sheet 3). Many of these (135 proteins, 101 thereof in both replicates) were ribosomal proteins or translation factors. We noted that of the remaining proteins, many are predicted to bind nucleic acids, such as tRNA synthetases or DNA-dependent RNA polymerases (Data S1, Sheet 3).

We considered a protein as potentially (indirectly) cGMP binding when it was detected with greater than or equal to two unique peptides in the cGMP-functionalized agarose beads in replicate but with maximally one unique peptide or an at least 10-fold lower intensity in the control bead replicates. Applying these constraints, 52 and 27 proteins were assigned as being retained in the 2-AH-cGMP and 2'-AHC-cGMP agarose beads, respectively (Data S1, Sheet 4). Of these, 17 proteins were present in both bead types. We included in the list of possible cGMP binders also four proteins that were eluted by 100 mM cGMP from either bead type (Data S1, Sheet 4).

In the 2-AH-cGMP bead fractions, we detected four proteins that are predicted to contain canonical cNMP-binding domains, namely, the cyclic nucleotide-binding (CNB) domain of the prokaryotic catabolite gene activator (or cAMP receptor protein) family (Rehmann et al., 2007) or the GAF (cGMP-dependent phosphodiesterases [PDEs], adenylyl cyclases, and FhIA) domains (Aravind & Ponting, 1997; Heikaus et al., 2009). CNB domains are often found in cNMP-dependent protein kinases, whereas the GAF domain is present, for example, in cNMP-regulated PDEs. Of the proteins that we assigned as possible cGMP binders, three are annotated as protein kinases with several CNB domains (Cre02.g076900.t1.1 [FAP19]; described in Wang et al., 2006, Cre12.g493250.t1.2 [FAP358]; and Cre16.g663200.t1.1 [FAP295]) and one as a GAF domain-containing PDE (Cre13.g605100.t1.2 [PDE20]). None of these four proteins were also captured by the 2'-AHC-cGMP beads (Data S1, Sheet 4).

Of the remaining possible cGMP binders, many proteins are known or predicted to bind nucleotides such as ADP or GTP, nucleotide derivatives such as S-adenosylmethionine (SAM) and NAD(P)H or nucleic acids (Data S1, Sheet 4). We were surprised that we found 15 enzymes known or predicted to be involved in starch metabolism in our compilation, none of which has a canonical cNMP-binding domain and most of which are not known to bind any nucleotides. All of these proteins were retained in the 2-AH-cGMP beads, and 10 of them in both beads, whereas none were only found in the 2'-AHC-cGMP beads.

We selected three enzymes from our list of possible cGMP binders to test for any effects this second messenger might exert on enzymatic activity. STA3 (Cre06.g282000; renamed SSS3A in the



Chlamydomonas v6.1 genome annotation), SBE1 (Cre06.g289850), and AMA2 (Cre08.g362450) were selected based on high peptide counts in the cGMP-functionalized beads. Additionally, *Chlamydomonas* mutants for STA3 (Ral et al., 2006, and references therein) and SBE1 (Tunçay et al., 2013) had been reported before, so that we hoped to be able to interconnect our biochemical with reported physiological data. In the case of AMA2, we were intrigued by the predicted presence of an N-terminal ACT domain, as these domains are known to allosterically regulate enzymes upon the binding of small ligands (Grant, 2006; Lang et al., 2014).

3.2 | Recombinant STA3, SBE1, and AMA2 showed the expected catalytic properties

Our target proteins were heterologously produced in *E. coli* and purified by *Strep*-tag affinity chromatography. The activities of SBE1 and AMA2 were determined by analyzing their effects on starch and, in the case of SBE1, amylopectin-iodine complexes, whereas STA3 activity was analyzed by a coupled enzyme assay (Kulichikhin et al., 2016). During the first experiments, we noted that all enzymes showed different specific activities depending on the amount of enzyme in the assay. Systematic testing of the optimal enzyme amounts revealed that SBE1 and STA3 were the most efficient in the

highest dilutions tested (.5 μg enzyme per assay; Figure S2). In the case of AMA2, low amounts of enzyme (.5 and 1 μg enzyme per assay) showed very high variability (Figure S2A), which we assumed to be due to unpredictable protein instability. Based on these tests, we routinely employed .5 μg (3.6 pmol) of recombinant STA3, .5 μg (5.7 pmol) of SBE1, and 2 μg (25.3 pmol) of AMA2 in 400 μL reaction mixtures. All enzymes showed the expected catalytic activities (Figures 1 and S2) in that the addition of AMA2 and SBE1 to starch or, in the case of SBE1, maize amylopectin resulted in a decrease of the absorption of the corresponding carbohydrate-iodine complexes. AMA2 and SBE1 activities were tested on soluble potato starch and on storage starch isolated from N-deficient *Chlamydomonas* cells. On soluble potato starch, AMA2 exhibited a specific activity of $73.4 \pm 1.4 \text{ U} \times \mu\text{mol}^{-1}$ and SBE1 of $467.1 \pm 62 \text{ U} \times \mu\text{mol}^{-1}$, and both enzymes showed similar activities on *Chlamydomonas* starch (Figure 1). On amylopectin, SBE1 developed an activity of $607.6 \pm 149.4 \text{ U} \times \mu\text{mol}^{-1}$ (Figure 1). STA3 activity in the presence of ADP-glucose and amylopectin resulted in the release of ADP as inferred from the generation of NADPH, and a specific activity of $529.3 \pm 140.8 \text{ U} \times \mu\text{mol}^{-1}$ was determined (Figure 1).

The specific activities of the enzymes were also analyzed at different pH values and temperatures to investigate whether they would be active within physiological ranges of these parameters. In the case of AMA2 and SBE1, the pH optima lay in the neutral region with a

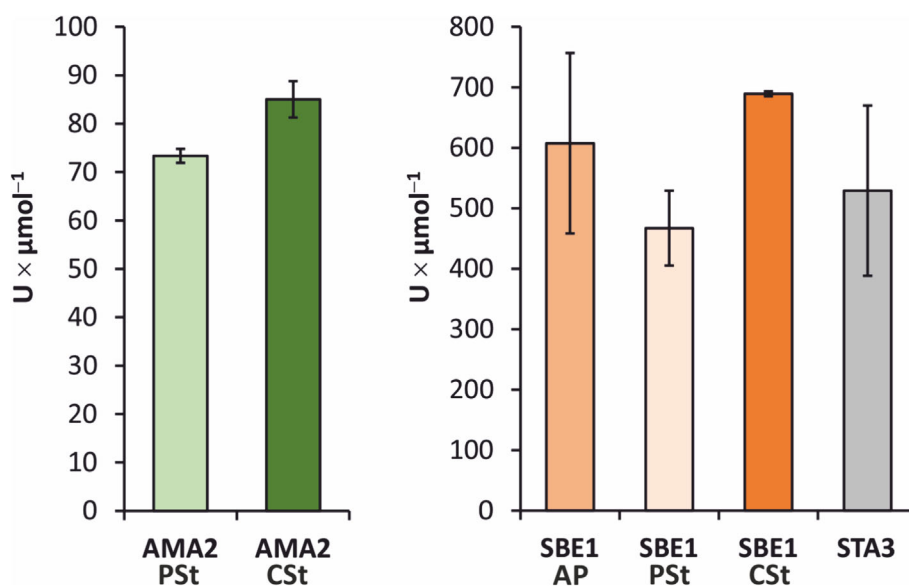


FIGURE 1 Recombinant AMA2, SBE1, and STA3 are active in vitro. In vitro activity assays were conducted employing 2 μg (25.3 pmol) of AMA2 and .5 μg of SBE1 (5.7 pmol) or STA3 (3.6 pmol). Amylase and starch-branching enzyme activities were determined on commercially available soluble potato starch (Pst), storage starch from N-deficient *Chlamydomonas* cells (Cst), or amylopectin (AP). AMA2 and SBE1 were diluted in 200 μL of “physiological buffer” (50 mM potassium phosphate, pH 7.4, 50 mM KCl, 10 mM NaCl, .5 mM MgCl₂, 100 nM CaCl₂), mixed with starch or amylopectin as indicated beneath the x-axes, and incubated for 30 min at 30°C. The reactions were quenched by adding HCl, and the absorption was determined at $\lambda = 580 \text{ nm}$ (starch) or $\lambda = 550 \text{ nm}$ (amylopectin) after adding iodine solution. Enzyme activity (U) was defined as the decrease of 1 mg of iodine-stainable substrate per minute. STA3 activity was determined by an assay developed by Kulichikhin et al. (2016). In this case, U was defined as the release of 1 μmol of adenosine diphosphate per minute. The columns show average values and error bars the standard deviation. The assays were conducted with three independent enzyme preparations in three independent experiments, except for AMA2 and SBE1 in the presence of *Chlamydomonas* starch, for which the columns show means of two independent experiments, conducted with two independent enzyme preparations.

tendency toward the alkaline (Figure S3A,B). AMA2 activity was optimal at pH 8 but still high at pH 7.5 and 8.5 (Figure S3A). SBE1 had a broad pH optimum profile on amylopectin and exhibited nearly the same activities from pH 6.5 to 7.5, while its activities at pH 6 and 8 were still high. On starch as substrate, it had a clearer optimum at pH 7.5 (Figure S3B). STA3 stood out in that its pH-dependent activity showed an optimum at pH 10. According to controls in which STA3 was replaced by ADP, the different buffer and pH values employed for the first reaction mixture did only slightly affect the subsequent enzymes of the assay (Figure S3C).

Temperature optima were determined for AMA2 and SBE1 and showed that both enzymes were active between 10°C and 50°C (Figure S4). Similar to the pH-dependent activities, temperature-dependent activity assays resulted in a steeper slope of the graph in the case of AMA2, with a temperature optimum at 40°C and a rather abrupt decrease of the specific activity at 45°C and 50°C (Figure S4A). SBE1 showed a broader temperature profile and had the highest activities at temperatures of 30°C, 35°C, and 40°C on amylopectin and an optimum at 30°C on starch as substrate (Figure S4B). On both substrates, SBE1 still showed rather high activities at 10°C and 45°C (Figure S4B).

3.3 | AMA2 activity decreased in the presence of the thiol-oxidant diamide

Several enzymes of the starch metabolism exhibit different activities in the presence of thiol-modifying redox agents or thioredoxins (Kötting et al., 2010; Santelia et al., 2015; Skryhan et al., 2018). We tested the effect of the disulfide reductant DTT and the thiol-oxidizing agent diamide on the enzymes analyzed here (Figure 2). The activities of SBE1 (Figure 2a) and STA3 (Figure 2b) did not change strongly after incubation with DTT or diamide. In contrast, AMA2 activity was notably impaired after incubation with diamide and decreased to $19.2 \pm 9.2\%$ and $7.2 \pm 2.7\%$ of the control activity after treatment with 1 and 5 mM diamide, respectively (Figure 2c). In the case of AMA2, we also tested whether its activity would be affected by the addition of calcium (Ca^{2+}) or the chelator EDTA (Figure 2d), because several α -amylases bind Ca^{2+} (e.g., Bush et al., 1989; Kadziola et al., 1994). The addition of Ca^{2+} to the standard activity assays did not result in enhanced AMA2 activities but, in contrast, to moderately decreased activities that reached $86.1 \pm 9.1\%$ of that of the control in the presence of 5 mM Ca^{2+} (Figure 2d). The presence of EDTA did only have a strong effect at a concentration of 10 mM, resulting in an AMA2 activity of $64.0 \pm 6.9\%$ relative to the control (Figure 2d).

3.4 | None of the enzymes analyzed here was directly affected by (cyclic) nucleotides

Because we had assigned the starch metabolism enzymes analyzed here as possible cGMP binders based on our cGMP affinity chromatography approach, we tested whether cGMP would influence their

activity. In neither case, an effect of the presence of 100 μM cGMP on enzymatic activity could be observed (Figure S5). We also tested cAMP, GMP, and AMP as well as c-di-GMP and guanosine tetraphosphate (ppGpp), because proteins regulated by cNMPs often show cross-reactivities such as in the case of cAMP- and cGMP-dependent protein kinases (Lorenz et al., 2017). The hyperphosphorylated guanosine nucleotide (p)ppGpp, originally described in prokaryotes, has a signaling function also in plants and algae (Field, 2018). Although a role of c-di-GMP in plants or algae has, to our knowledge, not been described, it regulates a glycogen-debranching enzyme in *Streptomyces venezuelae* (Schumacher et al., 2022). However, none of the additional nucleotides or nucleotide derivatives influenced the activities of AMA2, SBE1, or STA3 in the assays we employed during this work (Figure S5). In the case of STA3, a stimulating effect of AMP was very likely due to an impact on the subsequent enzymatic reactions, because it also resulted in a similarly enhanced NADPH generation when STA3 was replaced by ADP (Figure S5C).

3.5 | AMA2 activity was enhanced in the presence of Gln

Although we were unable to detect any direct effect on enzymatic activity by the tested nucleotides, we were still interested in the N-terminal ACT domain predicted for AMA2 because these domains are known for their interaction with small ligands (Grant, 2006; Lang et al., 2014). We first generated an AMA2 variant from which the N-terminal 269 amino acids were deleted, resulting in the α -amylase domain-only variant ΔAMA2 (Figure S1). The presence of variant ΔAMA2 decreased the absorption of starch-iodine complexes, and from the enzyme amounts tested, its optimal activity was reached when .5 μg (9.9 pmol) were employed (Figure S2A). Testing the activity of the ΔAMA2 variant at different pH values and temperatures showed that this α -amylase domain-only enzyme had similar pH and temperature optima as the full-length AMA2 enzyme (Figure 3a,b), although its pH profile around neutral pH (pH 7 to 8.5) was broader (Figure 3a). During these assays, we noted that at physiological pH values (Figure 3a) and at all temperatures tested (Figure 3b), the ΔAMA2 variant exhibited a roughly 2.8-fold higher specific activity than AMA2.

ACT domains are often found in enzymes involved in purine or amino acid metabolism, and they allosterically regulate the enzymatic function by binding intermediates or end products of the respective pathway (Liberles et al., 2005). We tested the effect of all proteinogenic amino acids on the activities of AMA2 and the N-terminally truncated variant ΔAMA2 (Figure 4; note that L-cysteine interfered with our assay and was therefore not included). The addition of L-arginine (Arg) and L-lysine (Lys) resulted in enhanced activities of both proteins to about 120% (AMA2) and 140% (ΔAMA2) (Figure 4). The effect of the presence of Gln stood out in that it resulted in an activity of full-length AMA2 of $168.2 \pm 2.4\%$ compared with the control reaction, while it hardly influenced the ACT domain-less ΔAMA2 variant whose activity reached $102.9 \pm 6.8\%$ of that of its control activity (Figure 4).

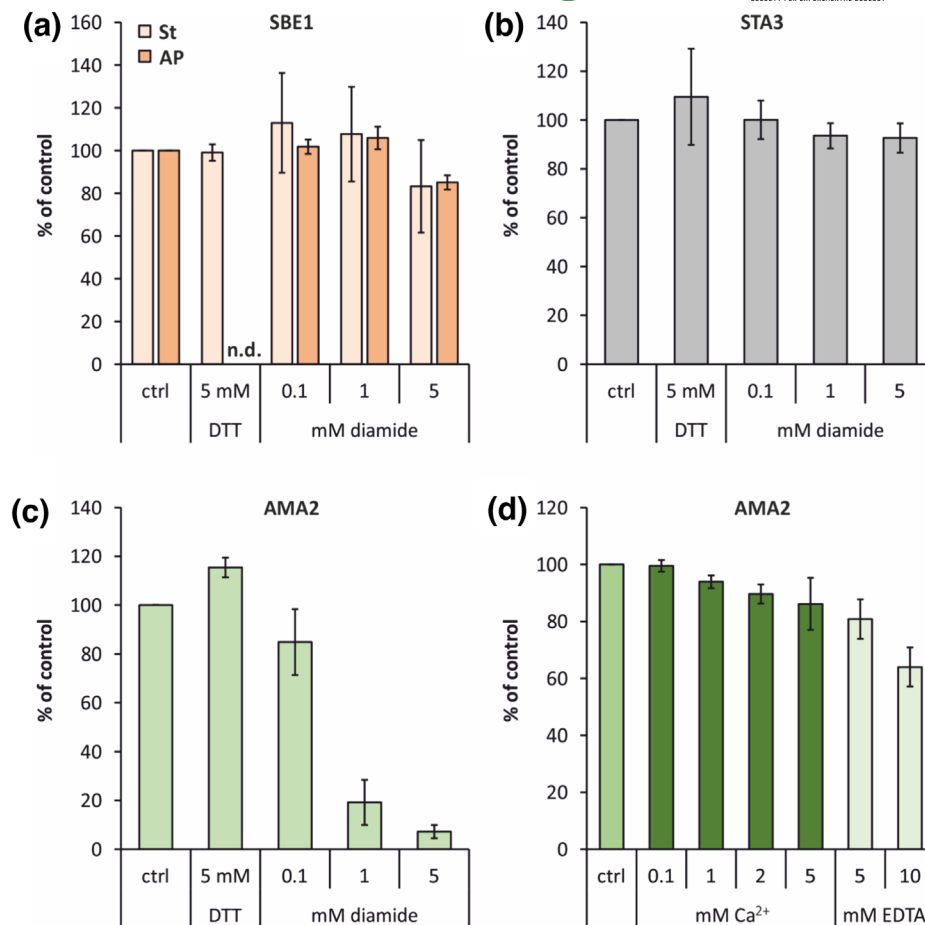


FIGURE 2 Effect of redox agents and calcium on enzyme activity. (a–c) The enzymes were diluted to concentrations of $1 \text{ mg} \times \text{mL}^{-1}$ in $20 \text{ }\mu\text{L}$ of “physiological buffer” containing the indicated concentrations of dithiothreitol (DTT) or diamide or, as controls (ctrl), no supplements. After incubating the samples for 20 min at 23°C , aliquots containing $2 \text{ }\mu\text{g}$ in the case of AMA2 and $.5 \text{ }\mu\text{g}$ in the case of SBE1 and STA3 were transferred to the standard activity assays that are described in detail in the caption of Figure 1. SBE1 activity was tested on both substrates, starch (St) and amylopectin (AP). (d) The effect of adding calcium (Ca^{2+}) or ethylenediaminetetraacetic acid (EDTA) on AMA2 activity was tested by adding the indicated concentrations directly to the standard activity assay as described in the caption of Figure 1. (a–d) For each independent experiment, the mean of technical triplicates (duplicates in the case of the STA3 assay) of the control reactions was set to 100%, and the activities determined in the presence of the supplements were calculated accordingly. The columns show mean values of at least two independent experiments and at least two independent protein preparations. Error bars show the standard deviations. The specific activities of the controls were (a) $462.9 \pm 83.7 \text{ U} \times \mu\text{mol}^{-1}$ (SBE1, St), $805.3 \pm 29.9 \text{ U} \times \mu\text{mol}^{-1}$ (SBE1, AP), (b) $473.8 \pm 26.8 \text{ U} \times \mu\text{mol}^{-1}$ (STA3), (c) $75.7 \pm 1.5 \text{ U} \times \mu\text{mol}^{-1}$ (AMA2), and (d) $59.9 \pm 15.7 \text{ U} \times \mu\text{mol}^{-1}$ (AMA2).

Testing the effect of the presence of different concentrations of Gln (.05 to 10 mM) on AMA2 activity and calculating dose response curves resulted in a half maximal effective concentration (EC_{50}) of Gln of $2.1 \pm .7 \text{ mM}$ (Figure 5a). Gln is a central intermediate and signaling molecule of the N assimilation pathway, and αKG has been recognized as an important signaling molecule at the intersection of N and C metabolism (Huergo & Dixon, 2015). We therefore tested whether αKG influenced AMA2 activity, either alone or in combination with Gln. However, this was not the case (Figure 5b).

ACT domains often form intermolecular or intramolecular interactions (Lang et al., 2014). We applied SEC to test the oligomeric state of AMA2 in comparison with that of the N-terminally truncated variant ΔAMA2 (Figure 6). Produced from the expression vector

employed here, recombinant AMA2 and ΔAMA2 have calculated sizes of 79.2 and 50.6 kDa, respectively. AMA2 eluted at a volume corresponding to a protein of 175 kDa, suggesting that it forms a dimer. According to its elution profile, the amylase domain-only variant ΔAMA2 was calculated to be a protein of 34 kDa, indicating that it was present as a monomer (Figure 6). In both cases, small shoulders preceding the main elution fractions suggested the formation of a small fraction of tetramers (AMA2) or dimers (ΔAMA2). The binding of ligands usually does not result in different oligomeric states of ACT domain-containing proteins but rather to conformational changes within the oligomer (Lang et al., 2014). We still tested whether the presence of a 10-fold molar excess of Gln would affect the elution profile of AMA2; however, this was not the case (Figure 6).

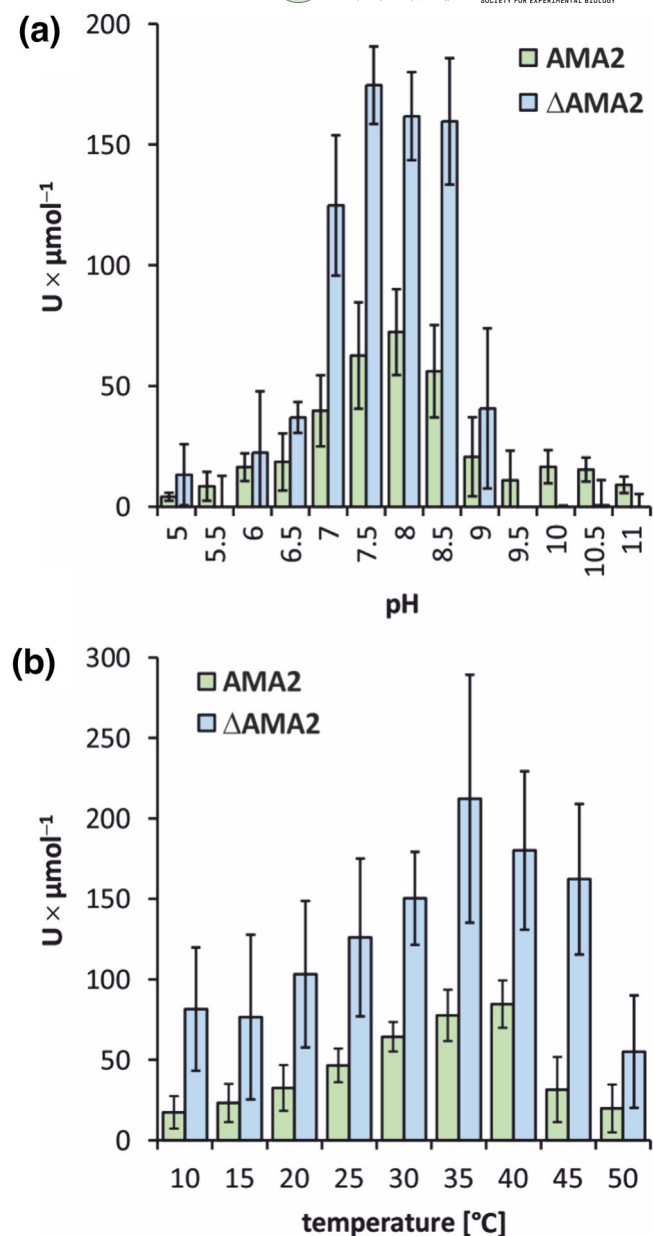


FIGURE 3 The α -amylase domain-only variant Δ AMA2 exhibits similar activity profiles as full-length AMA2. Amylase activities of AMA2 and the truncated variant Δ AMA2 were tested on commercially available soluble potato starch employing 2 μ g (25.3 pmol) of AMA2 or .5 μ g (9.9 pmol) of Δ AMA2. (a) To determine pH optima, the proteins were added to 200 μ L of Britton–Robinson buffer adjusted to the indicated pH values and mixed with 200 μ L starch solution, corresponding to 140 μ g of starch. After an incubation of 30 min at 30°C, the reaction was quenched by HCl, iodine solution was added, and the absorption was determined at $\lambda = 580$ nm. (b) Temperature optima were determined as described for (a), except that Britton–Robinson buffer, pH 7.5, was employed, and the incubation temperatures were adjusted as indicated at the x-axis. (a, b) Columns show average values, and error bars indicate the standard deviations. AMA2 data are the same as shown in Figures S3 and S4. Δ AMA2 data were obtained with two independent enzyme preparations in three (a) or four (b) independent experiments.

3.6 | Selected amino acid exchanges in the AMA2 ACT domain affect amylase activity and Gln sensitivity

The ACT domain of AMA2 appears to mediate the activating effect of Gln (Figure 4). We were interested to identify amino acids or parts of the ACT domain that would affect the Gln sensitivity of AMA2. The primary sequences of ACT domains are not well conserved (Aravind & Koonin, 1999; Liberles et al., 2005), which complicates the identification of key residues through comparisons with known ACT domains. To gain insights into how the ACT domain might fold, we modeled AMA2 as a dimer employing AlphaFold (note that an AlphaFold model of the AMA2 monomer is deposited in the AlphaFold Protein Structure Database under accession A0A2K3DGK5). Although the five models suggested by AlphaFold differed moderately, all showed the AMA2 dimer forming the shape of a fly, with the two ACT domains forming the “head” and the amylase domains forming the “wings” that are each connected by three α -helices to the ACT domains (Figure S6A).

To analyze α -amylase and ACT domain features in more detail, we employed the best-ranked AlphaFold model and PyMOL for visualization. We aligned the AMA2 model with the crystal structures of Barley α -amylase 1 (abbreviated as HvAMY1 in the following; protein data bank [PDB] accession 1HT6) (Robert et al., 2003) as well as Barley AMA2 in complex with the inhibitor acarbose (abbreviated as HvAMY2 in the following; PDB accession 1BG9) (Kadziola et al., 1998) (Figure S6). Additionally, we aligned the primary sequences employing Clustal Omega (Figure S7). The α -amylase domain of the AMA2 model superimposes both HvAMY1 and HvAMY2 structures well (Figure S6A,B). For example, the residues of the catalytic Asp–Glu–Asp triad (Kuriki & Imanaka, 1999, and references therein) overlies almost completely (Figure S6B, inset) and correspond to Asp476–Glu501–Asp584 of AMA2 (the numbering is according to the protein sequence Cre08.g362450.t1.2 including the N-terminal Met) (Figure S7). Two of the three structural Ca^{2+} -binding sites reported for both Barley α -amylases (Ca500 and Ca502 in PDB: 1HT6) (Robert et al., 2003, and references therein) appear conserved in the AMA2 model, although Lys435 would displace Ca500 (Figure S6C). The residues that bind the third Ca^{2+} , Ca501, are conserved neither in the structure model of AMA2 nor in its primary sequence (Figures S6D and S7).

Because of the effect of diamide on AMA2 activity (Figure 2c), we inspected its primary sequence and the AlphaFold model for Cys residues. The monomer contains nine Cys residues, two of which (Cys38 and Cys45) are located within the putative chloroplast targeting peptide (Figures S6A and S7). A third one (Cys97) is located before the second β -strand of the ACT domain (see below). Six Cys residues are located within the α -amylase domain, and Cys397 and Cys506, which lie near the active site, are visible on the surface of the AMA2 model (Figure S6E).

The ACT domain of AMA2 is predicted by AlphaFold to encompass residues 86 to 171 and to follow a $\beta\beta\alpha\beta\alpha$ topology (Figure S8A). Archetypical ACT domains of enzymes involved in amino acid metabolism mostly follow a $\beta\alpha\beta\alpha\beta$ topology (Lang et al., 2014), but different arrangements of α -helices and β -strands have been described. The

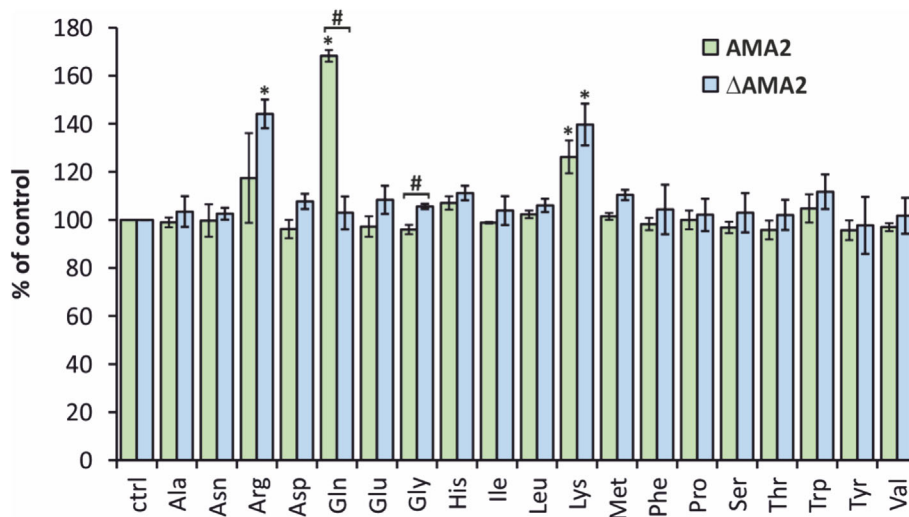


FIGURE 4 AMA2 activity is enhanced in the presence of L-glutamine. Activities of AMA2 (25.3 pmol) and the α -amylase domain-only variant Δ AMA2 (9.9 pmol) were determined as described in the caption of Figure 1, except that the indicated L-amino acids were added to the reaction mixtures to a concentration of 5 mM. The averages of technical triplicates of the control reactions that did not include an amino acid (ctrl) were set to 100% for each independent experiment, and the activities determined in the presence of individual amino acids were calculated in relation accordingly. Columns show mean values of at least two independent experiments, employing two independent protein preparations. Error bars show the standard deviations. The specific activities of the controls were $70.4 \pm 4.5 \text{ U} \times \mu\text{mol}^{-1}$ (AMA2) and $179.3 \pm 22.7 \text{ U} \times \mu\text{mol}^{-1}$ (Δ AMA2). Significant effects of single amino acids on either enzyme form are indicated by asterisks above individual bars. Significant differences between AMA2 and Δ AMA2 are indicated by brackets labeled by a hash sign. For both comparisons, significance was determined by analysis of variance followed by Tukey's honestly significant difference test (p -value ≤ 0.05).

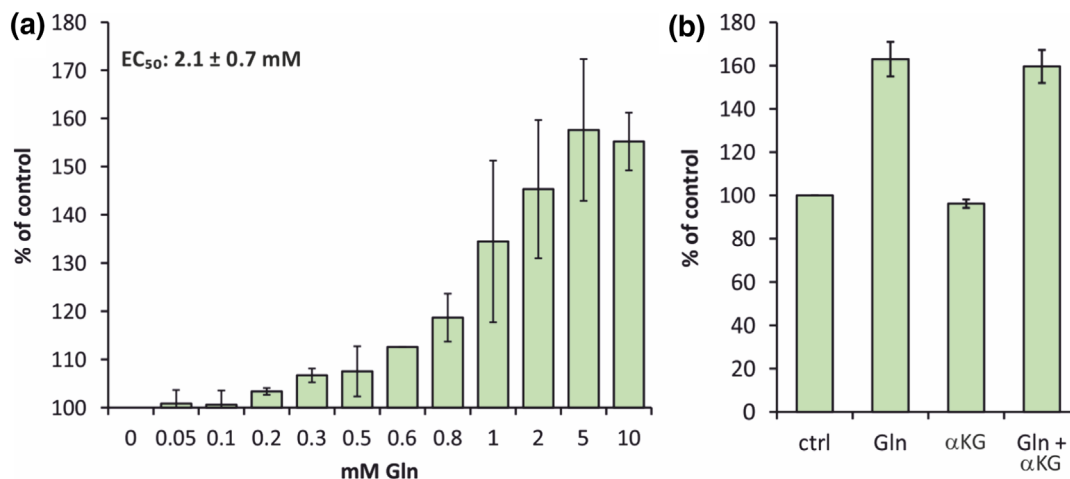


FIGURE 5 The effect of Gln on AMA2 activity is not altered in the presence of α -ketoglutarate. Activities of AMA2 (25.3 pmol) were analyzed as described in the caption of Figure 4, except that different concentrations of L-glutamine (Gln) were added to the reaction mixtures (a) or that α -ketoglutarate (α KG) was added to a final concentration of 5 mM either alone or together with 5 mM of Gln (b). (a) The effects of the indicated concentrations of Gln on AMA2 activity were tested in at least two independent experiments and at least two independent protein batches per concentration, but some concentrations were tested up to five times, using four enzyme preparations. A dose response curve was fitted employing the program OriginPro for each series independently, and the resulting values of the half maximal effective concentration (EC_{50}) were averaged. Note that the y-axis is scaled to begin at 100%. (b) The effect of the presence of Gln, α KG, or both on AMA2 activity was tested at least thrice, employing at least three independent enzyme preparations. (a, b) For each independent experiment, the specific activity of the control (ctrl), to which no supplement was added, was set to 100%, and the specific activities of reactions in the presence of Gln or α KG were calculated accordingly. The specific activities of the controls were $61.6 \pm 11.9 \text{ U} \times \mu\text{mol}^{-1}$ (a) and $67.4 \pm 6.7 \text{ U} \times \mu\text{mol}^{-1}$ (b).

$\beta\beta\alpha\beta\alpha$ topology is, for example, known from rat tyrosine hydroxylase (Zhang et al., 2014) or from ACT domains of several plant basic helix-loop-helix transcription factors (Feller et al., 2017; Lee et al., 2023).

The typical arrangement of four antiparallel β -strands and two antiparallel α -helices to one side of the β -sheet, however, is mostly conserved and also predicted for the AMA2 ACT domain (Figure S8A).

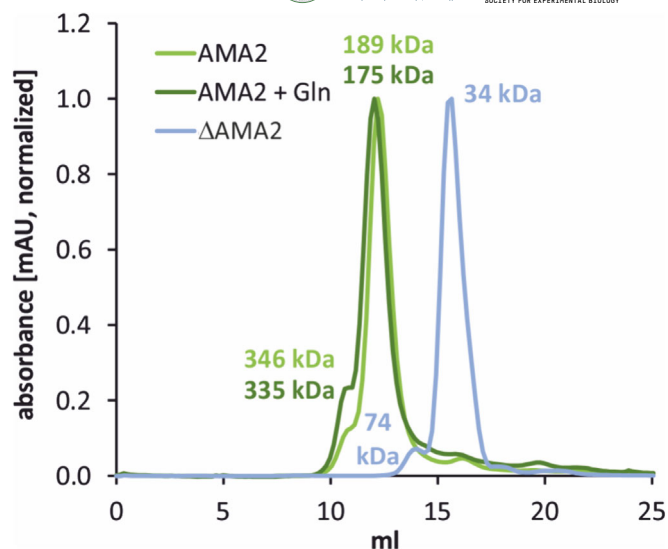


FIGURE 6 Recombinant AMA2 forms oligomers. Analytical size exclusion chromatography was performed to test for the oligomeric states of AMA2 and the α -amylase domain-only variant Δ AMA2. Proteins were diluted in Tris-HCl, pH 8, 150 mM NaCl, and loaded onto a Superdex 200 Increase 10/300 GL column with a 24 mL bed volume. Elution was done with the same buffer, and the absorbance of the eluate was recorded at $\lambda = 280$ nm. Normalized absorption profiles are shown. The molecular weights of the proteins present in the peaks were calculated according to a calibration performed employing a Gel Filtration Markers Kit. The elution profile of AMA2 was additionally tested in the presence of a 10-fold molar excess of L-glutamine (Gln). The molecular weights of the monomeric proteins as produced from the expression vectors are 79.2 kDa (AMA2) and 50.6 kDa (Δ AMA2).

Structures of ACT domain-containing proteins show that ACT domains mediate a multitude of oligomerizations (Grant, 2006; Lang et al., 2014). Often, ligands bind at interfaces of ACT domains, but they can also be coordinated by residues within a single ACT domain. One example for both modes is *Arabidopsis* Asp kinase, in which one effector, Lys, binds at the ACT domain interface and the other, SAM, binds within the ACT domain (Mas-Droux et al., 2006). Alignment methods suitable for the diverse primary sequences of ACT domains revealed conserved glycine (Gly) residues in loops between regions with secondary structures that, in some cases, were demonstrated to be involved in ligand binding (Grant, 2006, and references therein). A Gly-to-Asp exchange in *Arabidopsis* serine/threonine/tyrosine kinase 8 (STY8), for example, which is regulated by both isoleucine and SAM, results in a loss of sensitivity to isoleucine (Eisa et al., 2019). Inspecting the structure model of the AMA2 ACT domain, we identified three Gly residues in loops, namely, G122 (between α -helix 1 and β -strand 3), G135 (between β -strands 3 and 4), and G148 (between β -strand 4 and α -helix 2) (Figure S8B). AMA2 variants were generated in which these Gly residues were exchanged by Asp, and their activity was determined as described above for the wild-type enzyme both in the absence and presence of Gln. All variants had nearly the same specific activities as the wild-type protein, and their activities were increased in buffer containing Gln (Figure 7a). Variants G122D and G148D showed a similar

response to Gln as the wild-type enzyme. The increase of the activity of variant G135D was moderately stronger, reaching $210 \pm 11\%$ of its activity in the absence of Gln, although the difference to the wild-type enzyme was not statistically significant (Figure 7a).

We then decided to search for ACT domains with sequence homology to the AMA2 ACT domain to possibly identify conserved residues that might be important for its function. As described in detail in Section 2 and in the captions of Table S1 and Figure S9, we retrieved similar sequences employing NCBI's BlastP tool. Before generating the alignment, we manually added the ACT domain sequences of three proteins: *E. coli* GlnD is a uridylyltransferase/uridylyl-removing enzyme that modifies the P_{II} protein, a central signal transduction protein (Forchhammer et al., 2022), in response to Gln, for which the ACT domains of GlnD are required (Zhang et al., 2010). ACR11 is one of 12 so-called ACT repeat (ACR) proteins in *Arabidopsis* and is involved in the regulation of the GS/GOGAT cycle that assimilates ammonium and forms Gln (Liao et al., 2020, and references therein). We also added the ACT domain of *Chlamydomonas* starch phosphorylase STA4 (PhoB), which was also present in our cGMP affinity chromatography selection (Data S1, Sheet 4).

Inspecting the alignment but focusing on the ACT domain sequences of *E. coli* GlnD and *Arabidopsis* ACR11, we selected three additional residues that we exchanged in AMA2, namely, Asp106, Leu110, and Phe141 (the numbering is according to full-length AMA2). Residue Asp106 was found in both ACT domains each of *E. coli* GlnD and *Arabidopsis* ACR11 and is represented by Asp or Asn throughout our alignment (Figure S9). Leu110 is also quite conserved, being present in most of the sequences, whereas Phe141 is strictly conserved (Figure S9). According to our AlphaFold model, Asp106 and Leu110 are located at loop regions, whereas Phe141 reaches in the space between β -strand 4 and α -helix 1 (Figure S8C). Although the hydrophobic side chain of Phe is not intuitively associated with coordinating a polar amino acid, the aliphatic part of Gln is sandwiched between two Phe residues in a Gln-binding protein (Sun et al., 1998). The activity of the AMA2 variant D106F, in which Asp106 was exchanged by Phe, was very similar to that of the wild-type enzyme and it was still sensitive toward Gln (Figure 7b). The enzyme variants in which Leu110 and Phe141 were individually exchanged by Gly (L110G and F141G) showed impaired activities and contrary changes of activity in the presence of Gln: AMA2 L110G was almost insensitive to Gln, reaching $112 \pm 1\%$ of its activity determined in the absence of Gln, whereas the F141G variant was stimulated to $478 \pm 68\%$ of its standard activity when Gln was present in the assay (Figure 7b).

4 | DISCUSSION

4.1 | The enzymes analyzed here have mostly typical biochemical characteristics

The three enzymes that we picked from our cGMP affinity chromatography were detected in the *Chlamydomonas* chloroplast (Terashima et al., 2010), suggesting that they are involved in the plastid starch

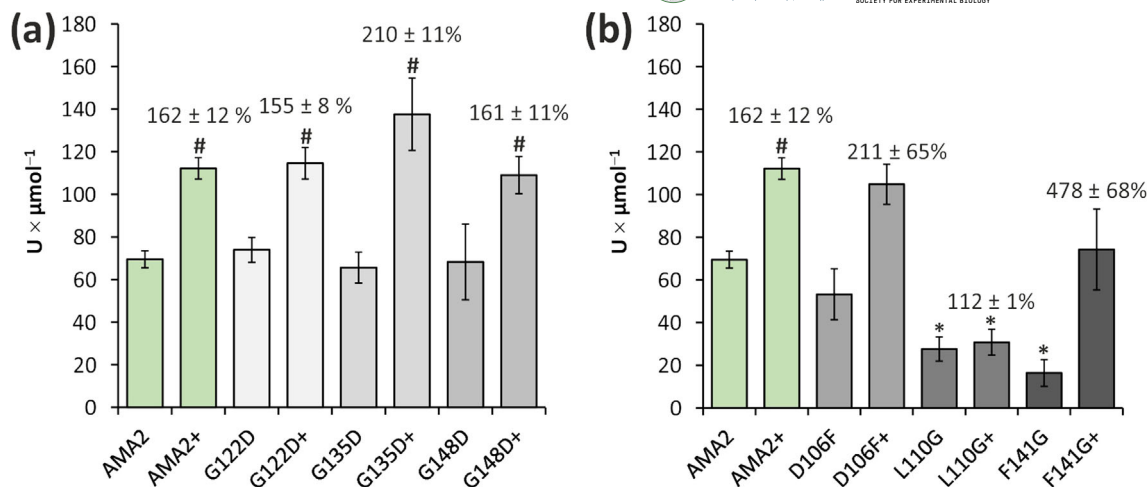


FIGURE 7 Amino acid exchanges in the AMA2 ACT domain have different effects on activity and Gln sensitivity. Activities of the AMA2 wild-type enzyme and single amino acid exchange variants were determined as described in the caption of Figure 4, both in the absence and presence of 5 mM of Gln (the latter is indicated by a plus sign after the variant denomination). Each enzyme variant was tested in at least two biological replicates and two independent experiments. Columns show the averages of the specific activities, and error bars indicate the standard deviation. For each variant, the relative activity determined in the presence of Gln compared with that in the absence of Gln was calculated and is indicated above the columns. (a) Activities of AMA2 variants in which glycine (G) residues within loops of the ACT domain were exchanged (see Figure S8B). (b) Activities of variants in which conserved residues identified by an alignment (Figure S9) were exchanged (depicted in Figure S8C). In (b), the results obtained with the wild-type enzyme are shown once more to facilitate a direct comparison. Significant differences between the activities of AMA2 variants and the wild-type enzyme, both in the absence or presence of Gln, are indicated by asterisks, and a significant effect of Gln on the activity of a given enzyme variant is indicated by a hash sign. Significance was analyzed by analysis of variance and a subsequent Tukey's honestly significant difference test (p -value ≤ 0.05).

metabolism of *Chlamydomonas*, and all showed the expected activities in their recombinant forms (Figure 1). The α -amylase AMA2 and the starch-branching enzyme SBE1 catalyzed changes to the starch or, in the case of SBE1, amylopectin substrate as indicated by the absorbance of polyglucan-iodine complexes. SBE1 was characterized in its recombinant form before and shown to be active on amylose (Courseaux et al., 2023). Both enzymes were also active on native *Chlamydomonas* storage starch, suggesting that they would be active in vivo on insoluble starch granules. The soluble starch synthase STA3 was capable of utilizing ADP-glucose as determined by the conversion of ADP to NADPH by subsequent enzymatic reactions in an assay developed previously (Kulichikhin et al., 2016). In the case of SBE1 and STA3, we noticed clear trends toward higher efficiencies when the enzymes were more dilute (Figure S2), which might simply be due to a better access of individual protein molecules to the polyglucan substrates. AMA2, however, revealed high standard deviations of its specific activities in higher dilutions (Figure S2). This suggests that the enzyme was unstable under these conditions. As we found recombinant AMA2 to be present as a dimer (see below; Figure 6), one possibility is that the complex dissociated at lower protein concentrations. In view of this behavior, we chose to employ higher concentrations of AMA2 in all activity assays, so that direct comparisons between full-length AMA2 and its N-terminally truncated variant Δ AMA2 (see below) need to be interpreted with caution.

AMA2 and SBE1 showed pH optima in the neutral region (Figure S3), although AMA2 revealed a steeper profile with a clear optimum at pH 8. This suggests that, in living *Chlamydomonas* cells,

AMA2 would be more active upon illumination when photosynthetic electron transport results in an alkalization of the chloroplast stroma (also see below). STA3 showed a broad pH profile with an optimum at pH 10 but still high activities at both pH 5 and 12 (Figure S3). High activities of soluble starch synthases in the alkaline region were noted before (e.g., Imparl-Radosevich et al., 1999). Although intracellular pH values are commonly in the neutral region, it is well possible that the microenvironment of starch synthases requires adaptability to different proton concentrations. In the case of *Chlamydomonas*, starch metabolism is additionally associated with the pyrenoid, a phase-separated compartment within the chloroplast responsible for CO₂ concentration. The pyrenoid is surrounded by starch sheaths, and proteomics have identified many starch metabolism enzymes in this sub-compartment (Lau et al., 2023; Mackinder et al., 2017; Zhan et al., 2018) (also see below). Indeed, SBE1 was present in the pyrenoid proteome (Zhan et al., 2018) and STA3 in the pyrenoid “proxosome” (Lau et al., 2023). The crowded environment of the liquid-like organelle might also result in (locally) different pH values.

4.2 | Starch metabolism enzymes might indirectly bind to cGMP

The activity of none of the enzymes we characterized here was influenced by the presence of cGMP or the other nucleotides tested (Figure S5), although the proteins were retained with high peptide counts in cGMP-functionalized agarose beads. This suggests that

either these enzymes bound unspecifically or that they were present because of interactions with other proteins. Principally, the approach was suitable to capture proteins that bind cNMPs. Of the 66 proteins we assigned as possible (indirect) cGMP binders (Data S1, Sheet 4), four are predicted to be typical cNMP-binding proteins in that they contain CNB or GAF domains (Aravind & Ponting, 1997; Heikaus et al., 2009; Rehmann et al., 2007). These proteins were only detected in the 2'-AH-cGMP and not in the 2'-AHC-cGMP bead fractions, suggesting that the former, to which the cGMP moiety is tethered through its C2 amine group, were better suited to capture canonical cNMP-binding proteins. Typically, cNMPs are mostly buried within GAF domains (Heikaus et al., 2009), and in mouse PDE2a, for example, only the C2 amino group of the guanosine base protrudes to the protein surface (Martinez et al., 2002) (Figure S10A). A larger part of cNMPs bound to CNB domains can be accessible from the protein surface; however, the ribose moiety projects toward the protein interior (e.g., Kim et al., 2016) (Figure S10B). This might hinder an efficient binding to the 2'-AHC-cGMP beads, in which the tether to the agarose material is attached at the 2' C-atom of the ribose moiety.

Of the remaining possible cGMP binders, many proteins are known or predicted to bind nucleotides, nucleotide derivatives or intermediates, or nucleic acids. Therefore, the proteins involved in starch metabolism captured by the cGMP-functionalized beads might have bound unspecifically. As noted in Section 1, starch metabolism enzymes can form multiprotein complexes (Abt & Zeeman, 2020; Geigenberger, 2011; Kötting et al., 2010; Schreier et al., 2019) so that it is possible that the proteins captured were bound to the beads through ADP-binding soluble starch synthases or an ATP-binding protein such as the alpha-glucan, water dikinase GWD2 (Data S1, Sheet 4). *Chlamydomonas* starch-branching enzymes were indeed detected in high-molecular weight complexes (Courseaux et al., 2023). In the case of SBE1 and STA3, possible protein partners were identified through high-throughput affinity purification approaches: SBE1 was affinity-purified by ribulose-1,5-bisphosphate carboxylase/oxygenase small subunit 2 and STA3 by SBE3 by Mackinder et al. (2017), and Wang et al. (2023) found SBE1 interacting with ribulose-1,5-bisphosphate carboxylase/oxygenase small subunit 1.

Alternatively, the starch metabolism enzymes detected in our cGMP interactome might have bound to the cGMP beads through an interaction with a cNMP-dependent protein kinase. We detected phosphorylated peptides of the three enzymes selected here in *Chlamydomonas* phosphoproteome studies (AMA2 and SBE1 in Shinkawa et al., 2019, and AMA2 and STA3 in Wang et al., 2014), demonstrating that they are phosphorylated in vivo. The *Chlamydomonas* genome encodes for several protein kinases with predicted CNB domains, three of which we detected in the 2'-AH-cGMP beads. FAP19 (Cre02.g076900) is involved in flagellar signaling (Wang et al., 2006), whereas FAP358 (Cre12.g493250) and FAP295 (Cre16.g663200) have, to our knowledge, not been analyzed yet. None of these three proteins is predicted to have a chloroplast targeting sequence. Notably, however, FAP358 and FAP295 were detected by the affinity purification approach of Mackinder et al. (2017) mentioned above. FAP358 was affinity-purified by the bicarbonate

transporter HLA3, the putatively chloroplastic acyl-carrier protein ACP2, and the thylakoid membrane bestrophin Cre16.g662600, although the scores (all <2.33) were much lower as the cut-off set by the authors for high-confidence interactions (>47.516). FAP295 was pulled down by NAR.2/LCIA, an anion transporter at the chloroplast membrane (score 32.76), also by HLA3 (score 28.89), by the CO₂ channel LCI1 (score 4.67), and also by bestrophin Cre16.g662600 (score 3.3). As HLA3 and LCI1 are plasma membrane transporters, both protein kinases were affinity-purified by both chloroplastic and plasma membrane proteins. Thus, although we find it intriguing to speculate on an interaction of cNMP-dependent protein kinases with starch metabolism enzymes, this idea will have to be tested in the future.

4.3 | AMA2 activity is enhanced by L-Gln through its ACT domain

When we started experiments on the selected starch metabolism enzymes, the N-terminal ACT domain of AMA2 was our first candidate for a possible interaction with cGMP. However, as none of the nucleotides tested here had an effect on AMA2 activity, we tested for an influence of proteinogenic amino acids, because these are common ligands of ACT domains (Eisa et al., 2019; Lang et al., 2014; Liberles et al., 2005). The α -amylase domain-only variant Δ AMA2 was tested in parallel to determine effects likely to exert influence through the ACT domain. Arg and Lys stimulated the activity of both proteins (Figure 4) so that these two amino acids probably had unspecific effects, for example, by enhancing the solubility of the proteins, although an effect on the α -amylase domain cannot be excluded. Gln, in contrast, only stimulated the activity of the full-length enzyme (Figure 4), suggesting that it exerts its effect through the ACT domain. In our assays, the variant Δ AMA2 showed higher specific activities (Figures S2 and S3) so that it may be hypothesized that the ACT domain has an inhibitory effect on α -amylase activity, which is released upon Gln binding. However, as discussed above, we assayed different protein amounts of AMA2 and Δ AMA2. Additionally, it is possible that the smaller Δ AMA2 variant simply had a better access to the starch substrate than the larger and dimeric (see below) AMA2 protein.

Both the AMA2 model in the AlphaFold Protein Structure Database (A0A2K3DGK5) and our AlphaFold model of an AMA2 dimer predict a typical ACT domain fold of the N-terminal region (Figures S6 and S8). Our gel filtration analyses indicate that full-length AMA2 forms at least a dimer, both in the absence and the presence of Gln, while the Δ AMA2 variant eluted as a monomer (Figure 6), suggesting that the ACT domain is involved in the oligomerization of AMA2. Notably, AMA2 was found to affinity purify itself in the abovementioned immunoprecipitation approach of Wang et al. (2023), corroborating our SEC elution profile. It is common that ACT domains mediate protein-protein interactions and that ligand binding changes the conformation of, but does not disintegrate, the oligomer (Grant, 2006; Lang et al., 2014). Also, the formation of an

eight-stranded β -sheet by the side-by-side arrangement of two ACT domains as predicted by our dimeric model was already observed in the first crystal structure of an ACT domain-containing protein (Schuller et al., 1995) and often since (Grant, 2006; Lang et al., 2014). Notably, however, in many cases, the α -helices face outward, which contrasts with our model (Figure S6). Whether this is the true AMA2 structure and, if so, whether it has a specific functional consequence will require future studies.

To identify the Gln-binding site within the AMA2 ACT domain, we generated six single amino-acid exchange variants based on comparisons with known and predicted ACT domains, the latter identified by homology searches (Table S1 and Figure S9). Neither AMA2 activity nor the stimulating effect of Gln was strongly affected by the exchanges of three Gly residues in loops (Figures 7a and S8B,C), suggesting that these residues are vital neither for the enzyme's active structure nor for the impact of Gln. However, the specific activities of variants with the exchanges D106F and particularly L110G and F141G were lower than that of the wild-type enzyme (Figure 7b). Additionally, the impact of Gln on the latter two variants varied strongly from that on the wild-type protein, albeit to opposite effects: The activity of variant L110G was rather insensitive to the presence of Gln, while that of variant F141G increased more than fourfold, although the latter was not statistically significant (Figure 7b). We hesitate to assign a Gln-coordinating function to L110G, because the impaired activity of this variant argues for a structural disturbance. However, all the latter three residues as well as G135, whose exchange resulted in a slightly stronger stimulating effect of Gln (Figure 7a), are located in or around a wedge-like shape formed between β -strands 3 and 4 and α -helix 1 (Figure S8A,C), suggesting that this is the region where Gln binds.

4.4 | Integration of starch degradation and Gln levels—A day in the life of *Chlamydomonas* R

The activating effect Gln exerts on AMA2 activity suggests that the α -amylase AMA2 might be a direct, enzymatic means to coordinate C and N metabolism in *Chlamydomonas* (Figure 8). In *Chlamydomonas* cells grown in day/night cycles, the starch content shows a rhythmic pattern. Depending on growth conditions (autotrophic or photomixotrophic), starch levels are the highest at the end of the subjective day or a few hours after the onset of darkness and decrease thereafter (Klein, 1987; Ral et al., 2006; Thyssen et al., 2001). In both autotrophic and mixotrophic growth conditions, net starch degradation usually continues well into the next light period (Klein, 1987; Ral et al., 2006; Strenkert et al., 2019; Thyssen et al., 2001), which was suggested to correlate with the cell cycle (Ral et al., 2006). *Chlamydomonas* cultures grown in regular dark/light cycles synchronize their cell cycle, exhibiting cell growth during the day and cell division in the beginning of the night (Bišová & Zachleder, 2014; Cross & Umen, 2015). Accordingly, cellular protein and chlorophyll contents increase during the day (Strenkert et al., 2019; Thyssen et al., 2001). RNA also accumulates rather constantly during the light phase, while the cellular DNA content increases toward the evening (Grant et al., 1978; Jüppner et al., 2017; Pokora et al., 2017). Nitrogen is present in considerable amounts in all of these molecules, and nitrate assimilation as well as ammonium fixation enzymes are indeed highly active during the day, although with different activity profiles: Both nitrate and nitrite reductases activities peak during the light phase, but whereas nitrate reductase is inactive during the night, nitrite reductase maintains a constant activity (Martínez-Rivas et al., 1991). The activities of GS and ferredoxin-dependent GOGAT (or glutamate

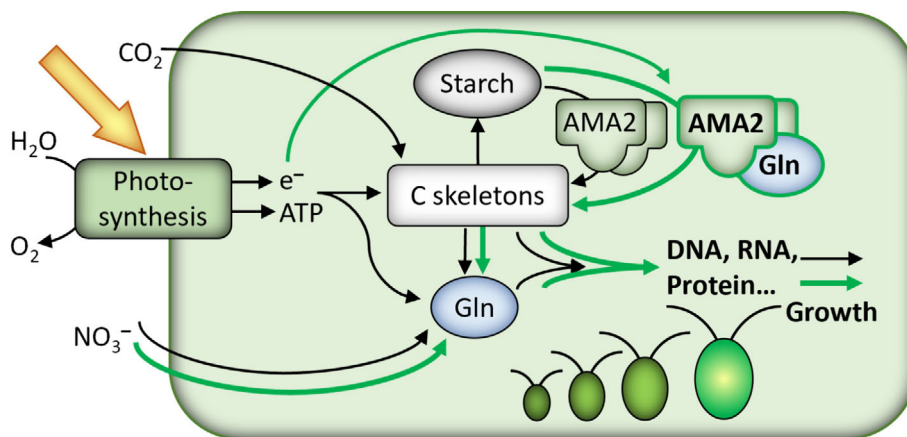


FIGURE 8 Schematic model of how the activating effect Gln exerts on AMA2 activity might allow a direct crosstalk between C and N metabolism to optimize cell growth. Photosynthesis provides energy (ATP) and reductant (e^-) to assimilate inorganic nutrients (only CO_2 and nitrate [NO_3^-] are shown). C and N are highly abundant in macromolecules such as DNA, RNA, and protein required for cell growth, which, in *Chlamydomonas*, occurs during the day. The dimeric α -amylase AMA2 is active under reducing conditions and might liberate C skeletons for biosynthetic pathways from transitory starch throughout the light period. High concentrations of the first N assimilation product, Gln, signal abundantly assimilated N. Through binding to the enzyme's ACT domain, Gln activates AMA2 further to stimulate the release of C skeletons to enhance the capacity for macromolecule synthesis. Black arrows indicate the highly simplified flow of molecules, and thick green arrows indicate stimulated pathways or processes.

synthase) increase constantly during the day and stay on a high level in the night (Martínez-Rivas et al., 1991). Glutamine, glutamate, and 2-oxoglutarate levels are higher during the light period, all three showing two maxima during the subjective day, but stay on relatively high levels during the night (Jüppner et al., 2017).

In view of these data, it seems reasonable to suggest that, during the day, *Chlamydomonas* coordinates N and C assimilation to efficiently biosynthesize N-containing molecules required for optimal cell growth. AMA2 could be one of the coordinating hubs, in that available N in the form of Gln stimulates its activity to release C skeletons (Figure 8). Our observations that recombinant AMA2 shows the highest activity at pH 8 (Figure S3) and is nearly inactive after pretreatment with the thiol-oxidizing agent diamide (Figure 2) support the notion that it might be mostly active during the day, similar to what has been observed for *Arabidopsis* α -amylase AMY3 and β -amylase BAM1 (Skryhan et al., 2018, and references therein). Reversible Cys reduction is employed by photosynthetic organisms to convey active photosynthetic electron transport to downstream sinks such as the CBB cycle, often by the thioredoxin system (Michelet et al., 2013). AMA2 contains several Cys residues (Figure S7) and was identified in a “thioredoxome” study (Pérez-Pérez et al. (2017); AMA2 is listed by its previous UniProt identifier A8J4D3), implying that the enzyme might be regulated through the thioredoxin system. Two of the Cys residues of AMA2 are located near the active site and appear solvent accessible as judged by viewing the surface of the AlphaFold AMA2 dimer model (Figure S6E). In the model, none of the Cys residues appear close enough to allow the formation of intramolecular or intermolecular disulfides; however, it is possible that the protein forms higher-order oligomers under oxidizing conditions or that only single Cys thiols are modified. AMA2 was indeed also identified by proteomics studies that captured S-glutathionylated (Zaffagnini et al., 2012) or S-nitrosylated proteins (Morisse et al., 2014) (in both studies, AMA2 can be found under its RefSeq identifier XP_001696014). It should be noted that the preceding argumentation is based on the hypothesis that AMA2 is located in the plastid. As mentioned above, AMA2 was detected in the chloroplast by proteomics (Terashima et al., 2010), and the localization prediction tool PredAlgo (Tardif et al., 2012) predicts a chloroplast targeting peptide (also see Figure S1). However, a recent high-throughput approach that employed fluorescent protein tagging detected AMA2 at the nuclear envelope (Wang et al., 2023). Although the authors discussed the possibility of mislocalizations, future studies of AMA2 need to pinpoint its localization(s).

5 | CONCLUSION

Our biochemical data indicate that the ACT domain of AMA2 functions as an amino acid sensor as has been demonstrated for many ACT domains before. We identified several putative α -amylases with N-terminal ACT domains in algae (Table S1), suggesting that the co-occurrence of these two domains is widespread in algae. We also detected a predicted N-terminal ACT domain in the *Chlamydomonas*

starch phosphorylase STA4 (PhoB), although its effect, if any, on phosphorylase activity has, to our knowledge, not been analyzed. STA4 appears to be solely involved in the accumulation of storage starch (Dauvillée et al., 2006), so that its ACT domain might fulfill another role as that in AMA2, which we hypothesize to be involved in starch degradation.

The ACT domain of AMA2 confers a specific activation of the enzyme by Gln, a central indicator for the N status. Gln also binds to the *Chlamydomonas* P_{II} protein and thereby indirectly relieves N-acetyl-L-glutamate kinase, which is central for polyamine and ornithine biosynthesis, from Arg feedback inhibition (Chellamuthu et al., 2014). Notably, the EC₅₀ value of $2.1 \pm .7$ mM of Gln we determined for AMA2 activation (Figure 5a) is close to the EC₅₀ of Gln Chellamuthu et al. (2014) determined for the activation of N-acetyl-L-glutamate kinase by the P_{II} protein ($2.4 \pm .8$ mM), suggesting that both regulatory effects might be operative under similar physiological conditions. Rather recently, it was shown that *Chlamydomonas* phosphoenolpyruvate carboxykinase isoform 2 is inhibited by Gln (Torresi et al., 2023), representing an additional example of a direct effect of Gln. It appears that the alga employs Gln as a signaling molecule to coordinate N and C metabolism directly at the enzymatic level in diverse contexts and that AMA2 might be an additional example.

AUTHOR CONTRIBUTIONS

L. S. and A. H. designed the research; L. S. performed the research; all authors analyzed the data; L. S. and A. H. wrote the first draft of the manuscript; and all authors edited the manuscript.

ACKNOWLEDGMENTS

We thank the Deutsche Forschungsgemeinschaft (DFG; German Research Foundation) for funding within RTG 2341 (Microbial Substrate Conversion [MiCon]; A. H. and E. H.). A. P. acknowledges funding from the German Federal Ministry of Education and Research, within the ERA-MIN2 framework, project MiCuR (O33RU011B). We are very thankful for excellent technical assistance and advice during the cGMP affinity chromatography experiments from M.Sc. Sabrina Duda (Photobiotechnology group, Ruhr University Bochum), Dr. Jan Lambertz (Department of Plant Biochemistry, Ruhr University Bochum), and Prof. Dr. Marc Nowaczyk (currently at the Department of Biochemistry, University of Rostock, Germany). Open Access funding enabled and organized by Projekt DEAL.

CONFLICT OF INTEREST STATEMENT

The authors declare no conflict of interest.

DATA AVAILABILITY STATEMENT

The data that support the findings of this study are available from the corresponding author, A. H., upon request.

ORCID

Lisa Scholtysek  <https://orcid.org/0009-0007-5678-195X>
 Ansgar Poetsch  <https://orcid.org/0000-0002-7540-3475>



Eckhard Hofmann <https://orcid.org/0000-0003-4874-372X>
Anja Hemschemeier <https://orcid.org/0000-0001-8879-3348>

REFERENCES

- Abt, M. R., & Zeeman, S. C. (2020). Evolutionary innovations in starch metabolism. *Current Opinion in Plant Biology*, 55, 109–117. <https://doi.org/10.1016/j.pbi.2020.03.001>
- Aravind, L., & Koonin, E. V. (1999). Gleaning non-trivial structural, functional and evolutionary information about proteins by iterative database searches. *Journal of Molecular Biology*, 287, 1023–1040. <https://doi.org/10.1006/jmbi.1999.2653>
- Aravind, L., & Ponting, C. P. (1997). The GAF domain: An evolutionary link between diverse phototransducing proteins. *Trends in Biochemical Sciences*, 22, 458–459. [https://doi.org/10.1016/s0968-0004\(97\)01148-1](https://doi.org/10.1016/s0968-0004(97)01148-1)
- Asatsuma, S., Sawada, C., Itoh, K., Okito, M., Kitajima, A., & Mitsui, T. (2005). Involvement of α -amylase I-1 in starch degradation in rice chloroplasts. *Plant & Cell Physiology*, 46, 858–869. <https://doi.org/10.1093/pcp/pci091>
- Bertoft, E. (2017). Understanding starch structure: Recent progress. *Agronomy*, 7, 56. <https://doi.org/10.3390/agronomy7030056>
- Bišová, K., & Zachleder, V. (2014). Cell-cycle regulation in green algae dividing by multiple fission. *Journal of Experimental Botany*, 65, 2585–2602. <https://doi.org/10.1093/jxb/ert466>
- Britton, H. T. S., & Robinson, R. A. (1931). CXC VIII.—Universal buffer solutions and the dissociation constant of veronal. *Journal of the Chemical Society*, 0, 1456–1462. <https://doi.org/10.1039/JR9310001456>
- Bush, D. S., Sticher, L., van Huystee, R., Wagner, D., & Jones, R. L. (1989). The calcium requirement for stability and enzymatic activity of two isoforms of barley aleurone α -amylase. *The Journal of Biological Chemistry*, 264, 19392–19398. [https://doi.org/10.1016/S0021-9258\(19\)47314-6](https://doi.org/10.1016/S0021-9258(19)47314-6)
- Calatrava, V., Tejada-Jimenez, M., Sanz-Luque, E., Fernandez, E., & Galvan, A. (2023). Chapter 3—Nitrogen metabolism in *Chlamydomonas*. In A. R. Grossman & F.-A. Wollman (Eds.), *The Chlamydomonas sourcebook* (Third ed.) (pp. 99–128). Academic Press. <https://doi.org/10.1016/B978-0-12-821430-5.00004-3>
- Chellamuthu, V. R., Ermilova, E., Lapina, T., Lüddecke, J., Minaeva, E., Herrmann, C., Hartmann, M. D., & Forchhammer, K. (2014). A widespread glutamine-sensing mechanism in the plant kingdom. *Cell*, 159, 1188–1199. <https://doi.org/10.1016/j.cell.2014.10.015>
- Cormann, K. U., Möller, M., & Nowaczyk, M. M. (2016). Critical assessment of protein cross-linking and molecular docking: An updated model for the interaction between photosystem II and Psb27. *Frontiers in Plant Science*, 7, 157. <https://doi.org/10.3389/fpls.2016.00157>
- Courseaux, A., George, O., Deschamps, P., Bompard, C., Duchêne, T., & Dauvillée, D. (2023). BE3 is the major branching enzyme isoform required for amylopectin synthesis in *Chlamydomonas reinhardtii*. *Frontiers in Plant Science*, 14, 1201386. <https://doi.org/10.3389/fpls.2023.1201386>
- Critchley, J. H., Zeeman, S. C., Takaha, T., Smith, A. M., & Smith, S. M. (2001). A critical role for disproportionating enzyme in starch breakdown is revealed by a knock-out mutation in *Arabidopsis*. *The Plant Journal*, 26, 89–100. <https://doi.org/10.1046/j.1365-313x.2001.01012.x>
- Cross, F. R., & Umen, J. G. (2015). The *Chlamydomonas* cell cycle. *The Plant Journal*, 82, 370–392. <https://doi.org/10.1111/tpj.12795>
- Dauvillée, D., Chochois, V., Steup, M., Haebel, S., Eckermann, N., Ritte, G., Ral, J. P., Colleoni, C., Hicks, G., Wattebled, F., Deschamps, P., D'Hulst, C., Liénard, L., Cournac, L., Putaux, J. L., Dupeyre, D., & Ball, S. G. (2006). Plastidial phosphorylase is required for normal starch synthesis in *Chlamydomonas reinhardtii*. *The Plant Journal*, 48, 274–285. <https://doi.org/10.1111/j.1365-313X.2006.02870.x>
- Delrue, B., Fontaine, T., Routier, F., Decq, A., Wieruszkeski, J. M., Van Den Koornhuysse, N., Maddelein, M. L., Fournet, B., & Ball, S. (1992). Waxy *Chlamydomonas reinhardtii*: Monocellular algal mutants defective in amylose biosynthesis and granule-bound starch synthase activity accumulate a structurally modified amylopectin. *Journal of Bacteriology*, 174, 3612–3620. <https://doi.org/10.1128/jb.174.11.3612-3620.1992>
- Deschamps, P., Ball, S. G., & Dauvillée, D. (2023). The comparative, biochemistry, genetics, and evolution of starch metabolism in *Chlamydomonas reinhardtii*. In A. R. Grossman & F.-A. Wollman (Eds.), *The Chlamydomonas sourcebook* (Third ed.) (pp. 23–50). Academic Press. <https://doi.org/10.1016/B978-0-12-821430-5.00003-1>
- Donaldson, L., & Meier, S. (2013). An affinity pull-down approach to identify the plant cyclic nucleotide interactome. *Methods in Molecular Biology*, 1016, 155–173. https://doi.org/10.1007/978-1-62703-441-8_11
- Donaldson, L., Meier, S., & Gehring, C. (2016). The Arabidopsis cyclic nucleotide interactome. *Cell Communication and Signaling: CCS*, 14, 10. <https://doi.org/10.1186/s12964-016-0133-2>
- Düner, M., Lambert, J., Mügge, C., & Hemschemeier, A. (2018). The soluble guanylate cyclase CYG12 is required for the acclimation to hypoxia and trophic regimes in *Chlamydomonas reinhardtii*. *The Plant Journal*, 93, 311–337. <https://doi.org/10.1111/tpj.13779>
- Eisa, A., Bölter, B., & Schwenkert, S. (2019). The ACT domain in chloroplast precursor-phosphorylating STY kinases binds metabolites and allosterically regulates kinase activity. *The Journal of Biological Chemistry*, 294, 17278–17288. <https://doi.org/10.1074/jbc.RA119.010298>
- Evans R, O'Neill M, Pritzel A, Antropova N, Senior A, Green T, Židek A, Bates R, Blackwell S, Yim J, et al. (2022) Protein complex prediction with AlphaFold-multimer. bioRxiv:2021.2010.2004.463034. <https://doi.org/10.1101/2021.10.04.463034>
- Feller, A., Yuan, L., & Grotewold, E. (2017). The BIF domain in plant bHLH proteins is an ACT-like domain. *Plant Cell*, 29, 1800–1802. <https://doi.org/10.1105/tpc.17.00356>
- Field, B. (2018). Green magic: Regulation of the chloroplast stress response by (p)ppGpp in plants and algae. *Journal of Experimental Botany*, 69, 2797–2807. <https://doi.org/10.1093/jxb/erx485>
- Figueroa, C. M., Asencion Diez, M. D., Ballicora, M. A., & Iglesias, A. A. (2022). Structure, function, and evolution of plant ADP-glucose pyrophosphorylase. *Plant Molecular Biology*, 108, 307–323. <https://doi.org/10.1007/s11103-021-01235-8>
- Forchhammer, K., Selim, K. A., & Huergo, L. F. (2022). New views on PII signaling: From nitrogen sensing to global metabolic control. *Trends in Microbiology*, 30, 722–735. <https://doi.org/10.1016/j.tim.2021.12.014>
- Franzén, L. G., Rochaix, J. D., & von Heijne, G. (1990). Chloroplast transit peptides from the green alga *Chlamydomonas reinhardtii* share features with both mitochondrial and higher plant chloroplast presequences. *FEBS Letters*, 260, 165–168. [https://doi.org/10.1016/0014-5793\(90\)80094-y](https://doi.org/10.1016/0014-5793(90)80094-y)
- Geigenberger, P. (2011). Regulation of starch biosynthesis in response to a fluctuating environment. *Plant Physiology*, 155, 1566–1577. <https://doi.org/10.1104/pp.110.170399>
- Grant, D., Swinton, D. C., & Chiang, K. S. (1978). Differential patterns of mitochondrial, chloroplast and nuclear DNA synthesis in the synchronous cell cycle of *Chlamydomonas reinhardtii*. *Planta*, 141, 259–267. <https://doi.org/10.1007/BF00388341>
- Grant, G. A. (2006). The ACT domain: A small molecule binding domain and its role as a common regulatory element. *The Journal of Biological Chemistry*, 281, 33825–33829. <https://doi.org/10.1074/jbc.R600024200>
- Guan, H. P., & Preiss, J. (1993). Differentiation of the properties of the branching isozymes from maize (*Zea mays*). *Plant Physiology*, 102, 1269–1273. <https://doi.org/10.1104/pp.102.4.1269>

- Harris, E. H. (1989). *The Chlamydomonas sourcebook: A comprehensive guide to biology and laboratory use*. Academic Press. <https://doi.org/10.1016/C2009-0-02778-0>
- Heikau, C. C., Pandit, J., & Klevit, R. E. (2009). Cyclic nucleotide binding GAF domains from phosphodiesterases: Structural and mechanistic insights. *Structure*, 17, 1551–1557. <https://doi.org/10.1016/j.str.2009.07.019>
- Huergo, L. F., & Dixon, R. (2015). The emergence of 2-oxoglutarate as a master regulator metabolite. *Microbiology and Molecular Biology Reviews*, 79, 419–435. <https://doi.org/10.1128/MMBR.00038-15>
- Huwald, D., Schrapers, P., Kositzki, R., Haumann, M., & Hemschemeier, A. (2015). Characterization of unusual truncated hemoglobins of *Chlamydomonas reinhardtii* suggests specialized functions. *Planta*, 242, 167–185. <https://doi.org/10.1007/s00425-015-2294-4>
- Hwang, S. K., Nishi, A., Satoh, H., & Okita, T. W. (2010). Rice endosperm-specific plastidial alpha-glucan phosphorylase is important for synthesis of short-chain malto-oligosaccharides. *Archives of Biochemistry and Biophysics*, 495, 82–92. <https://doi.org/10.1016/j.abb.2009.12.023>
- Imparl-Radosevich, J. M., Nichols, D. J., Li, P., McKean, A. L., Keeling, P. L., & Guan, H. (1999). Analysis of purified maize starch synthases IIa and IIb: SS isoforms can be distinguished based on their kinetic properties. *Archives of Biochemistry and Biophysics*, 362, 131–138. <https://doi.org/10.1006/abbi.1998.1028>
- Irshad, A., Guo, H., Rehman, S. U., Wang, X., Wang, C., Raza, A., Zhou, C., Li, Y., & Liu, L. (2021). Soluble starch synthase enzymes in cereals: An updated review. *Agronomy*, 11, 1983. <https://doi.org/10.3390/agronomy11101983>
- Jumper, J., Evans, R., Pritzel, A., Green, T., Figurnov, M., Ronneberger, O., Tunyasuvunakool, K., Bates, R., Židek, A., Potapenko, A., Bridgland, A., Meyer, C., Kohl, S. A. A., Ballard, A. J., Cowie, A., Romera-Paredes, B., Nikolov, S., Jain, R., Adler, J., ... Hassabis, D. (2021). Highly accurate protein structure prediction with AlphaFold. *Nature*, 596, 583–589. <https://doi.org/10.1038/s41586-021-03819-2>
- Jüppner, J., Mubeen, U., Lisse, A., Caldana, C., Brust, H., Steup, M., Herrmann, M., Steinhauser, D., & Giavalisco, P. (2017). Dynamics of lipids and metabolites during the cell cycle of *Chlamydomonas reinhardtii*. *The Plant Journal*, 92, 331–343. <https://doi.org/10.1111/tj.13642>
- Kadziola, A., Abe, J., Svensson, B., & Haser, R. (1994). Crystal and molecular structure of barley α -amylase. *Journal of Molecular Biology*, 239, 104–121. <https://doi.org/10.1006/jmbi.1994.1354>
- Kadziola, A., Søgaard, M., Svensson, B., & Haser, R. (1998). Molecular structure of a barley α -amylase-inhibitor complex: Implications for starch binding and catalysis. *Journal of Molecular Biology*, 278, 205–217. <https://doi.org/10.1006/jmbi.1998.1683>
- Kim, E., & Park, J. M. (2003). Identification of novel target proteins of cyclic GMP signaling pathways using chemical proteomics. *Journal of Biochemistry and Molecular Biology*, 36, 299–304. <https://doi.org/10.5483/bmbrep.2003.36.3.299>
- Kim, J. J., Lorenz, R., Arold, S. T., Reger, A. S., Sankaran, B., Casteel, D. E., Herberg, F. W., & Kim, C. (2016). Crystal structure of PKG I:cGMP complex reveals a cGMP-mediated dimeric interface that facilitates cGMP-induced activation. *Structure*, 24, 710–720. <https://doi.org/10.1016/j.str.2016.03.009>
- Klein, U. (1987). Intracellular carbon partitioning in *Chlamydomonas reinhardtii*. *Plant Physiology*, 85, 892–897. <https://doi.org/10.1104/pp.85.4.892>
- Kötting, O., Kossmann, J., Zeeman, S. C., & Lloyd, J. R. (2010). Regulation of starch metabolism: The age of enlightenment? *Current Opinion in Plant Biology*, 13, 321–329. <https://doi.org/10.1016/j.pbi.2010.01.003>
- Kulichikhin, K., Mukherjee, S., & Ayele, B. T. (2016). Extraction and assays of ADP-glucose pyrophosphorylase, soluble starch synthase and granule bound starch synthase from wheat (*Triticum aestivum* L.) grains. *Bio-Protocol*, 6, e1929. <https://doi.org/10.21769/BioProtoc.1929>
- Kuriki, T., & Imanaka, T. (1999). The concept of the α -amylase family: Structural similarity and common catalytic mechanism. *Journal of Biochemistry and Bioengineering*, 87, 557–565. [https://doi.org/10.1016/s1389-1723\(99\)80114-5](https://doi.org/10.1016/s1389-1723(99)80114-5)
- Lang, E. J., Cross, P. J., Mittelstädt, G., Jameson, G. B., & Parker, E. J. (2014). Allosteric ACTin: The varied ACT domains regulating enzymes of amino-acid metabolism. *Current Opinion in Structural Biology*, 29, 102–111. <https://doi.org/10.1016/j.sbi.2014.10.007>
- Lau, C. S., Dowie, A., Thomas, G. H., Girr, P., & Mackinder, L. C. M. (2023). A phase-separated CO₂-fixing pyrenoid proteome determined by TurboID in *Chlamydomonas reinhardtii*. *Plant Cell*, 35, 3260–3279. <https://doi.org/10.1093/plcell/koad131>
- Lee, Y. S., Shiu, S. H., & Grotewold, E. (2023). Evolution and diversification of the ACT-like domain associated with plant basic helix-loop-helix transcription factors. *Proceedings of the National Academy of Sciences of the United States of America*, 120, e2219469120. <https://doi.org/10.1073/pnas.2219469120>
- Levi, C., & Gibbs, M. (1984). Starch degradation in synchronously grown *Chlamydomonas reinhardtii* and characterization of the amylase. *Plant Physiology*, 74, 459–463. <https://doi.org/10.1104/pp.74.3.459>
- Li, J., Zhou, W., Francisco, P., Wong, R., Zhang, D., & Smith, S. M. (2017). Inhibition of *Arabidopsis* chloroplast β -amylase BAM3 by maltotriose suggests a mechanism for the control of transitory leaf starch mobilization. *PLoS ONE*, 12, e0172504. <https://doi.org/10.1371/journal.pone.0172504>
- Liao, H. S., Chung, Y. H., Chardin, C., & Hsieh, M. H. (2020). The lineage and diversity of putative amino acid sensor ACR proteins in plants. *Amino Acids*, 52, 649–666. <https://doi.org/10.1007/s00726-020-02844-1>
- Liberles, J. S., Thórolfsson, M., & Martínez, A. (2005). Allosteric mechanisms in ACT domain containing enzymes involved in amino acid metabolism. *Amino Acids*, 28, 1–12. <https://doi.org/10.1007/s00726-004-0152-y>
- Liu, X., Hu, B., & Chu, C. (2022). Nitrogen assimilation in plants: Current status and future prospects. *Journal of Genetics and Genomics*, 49, 394–404. <https://doi.org/10.1016/j.jgg.2021.12.006>
- Lorenz, R., Bertinetti, D., & Herberg, F. W. (2017). cAMP-dependent protein kinase and cGMP-dependent protein kinase as cyclic nucleotide effectors. *Handbook of Experimental Pharmacology*, 238, 105–122. https://doi.org/10.1007/164_2015_36
- Lu, K. J., Pfister, B., Jenny, C., Eicke, S., & Zeeman, S. C. (2018). Distinct functions of STARCH SYNTHASE 4 domains in starch granule formation. *Plant Physiology*, 176, 566–581. <https://doi.org/10.1104/pp.17.01008>
- Mackinder, L. C. M., Chen, C., Leib, R. D., Patena, W., Blum, S. R., Rodman, M., Ramundo, S., Adams, C. M., & Jonikas, M. C. (2017). A spatial Interactome reveals the protein organization of the algal CO₂-concentrating mechanism. *Cell*, 171(133–147), e114. <https://doi.org/10.1016/j.cell.2017.08.044>
- Martinez, S. E., Wu, A. Y., Glavas, N. A., Tang, X. B., Turley, S., Hol, W. G., & Beavo, J. A. (2002). The two GAF domains in phosphodiesterase 2A have distinct roles in dimerization and in cGMP binding. *Proceedings of the National Academy of Sciences of the United States of America*, 99, 13260–13265. <https://doi.org/10.1073/pnas.192374899>
- Martínez-Rivas, J. M., Vega, J. M., & Márquez, A. J. (1991). Differential regulation of the nitrate-reducing and ammonium-assimilatory systems in synchronous cultures of *Chlamydomonas reinhardtii*. *FEMS Microbiology Letters*, 78, 85–88. <https://doi.org/10.1111/j.1574-6968.1991.tb04422.x>
- Mas-Droux, C., Curien, G., Robert-Genthon, M., Laurencin, M., Ferrer, J. L., & Dumas, R. (2006). A novel organization of ACT



- domains in allosteric enzymes revealed by the crystal structure of *Arabidopsis* aspartate kinase. *Plant Cell*, 18, 1681–1692. <https://doi.org/10.1105/tpc.105.040451>
- Mehrpouyan, S., Menon, U., Tetlow, I. J., & Emes, M. J. (2021). Protein phosphorylation regulates maize endosperm starch synthase IIa activity and protein–protein interactions. *The Plant Journal*, 105, 1098–1112. <https://doi.org/10.1111/tbj.15094>
- Michelet, L., Zaffagnini, M., Morisse, S., Sparla, F., Pérez-Pérez, M. E., Francia, F., Danon, A., Marchand, C. H., Fermani, S., Trost, P., & Lemaire, S. D. (2013). Redox regulation of the Calvin-Benson cycle: Something old, something new. *Frontiers in Plant Science*, 4, 470. <https://doi.org/10.3389/fpls.2013.00470>
- Mikkelsen, R., Mutenda, K. E., Mant, A., Schurmann, P., & Blennow, A. (2005). α -Glucan, water dikinase (GWD): A plastidic enzyme with redox-regulated and coordinated catalytic activity and binding affinity. *Proceedings of the National Academy of Sciences of the United States of America*, 102, 1785–1790. <https://doi.org/10.1073/pnas.0406674102>
- Mirdita, M., Schütze, K., Moriwaki, Y., Heo, L., Ovchinnikov, S., & Steinegger, M. (2022). ColabFold: Making protein folding accessible to all. *Nature Methods*, 19, 679–682. <https://doi.org/10.1038/s41592-022-01488-1>
- Morisse, S., Zaffagnini, M., Gao, X. H., Lemaire, S. D., & Marchand, C. H. (2014). Insight into protein S-nitrosylation in *Chlamydomonas reinhardtii*. *Antioxidants & Redox Signaling*, 21, 1271–1284. <https://doi.org/10.1089/ars.2013.5632>
- Paysan-Lafosse, T., Blum, M., Chuguransky, S., Grego, T., Pinto, B. L., Salazar, G. A., Bileschi, M. L., Bork, P., Bridge, A., Colwell, L., Gough, J., Haft, D. H., Letunić, I., Marchler-Bauer, A., Mi, H., Natale, D. A., Orengo, C. A., Pandurangan, A. P., Rivoire, C., ... Bateman, A. (2023). InterPro in 2022. *Nucleic Acids Research*, 51, D418–D427. <https://doi.org/10.1093/nar/gkac993>
- Pérez-Pérez, M. E., Mauriès, A., Maes, A., Tourasse, N. J., Hamon, M., Lemaire, S. D., & Marchand, C. H. (2017). The deep thioredoxome in *Chlamydomonas reinhardtii*: New insights into redox regulation. *Molecular Plant*, 10, 1107–1125. <https://doi.org/10.1016/j.molp.2017.07.009>
- Pfister, B., & Zeeman, S. C. (2016). Formation of starch in plant cells. *Cellular and Molecular Life Sciences*, 73, 2781–2807. <https://doi.org/10.1007/s00018-016-2250-x>
- Pokora, W., Aksmann, A., Baścik-Remisiewicz, A., Dettlaff-Pokora, A., Rykaczewski, M., Gappa, M., & Tukaj, Z. (2017). Changes in nitric oxide/hydrogen peroxide content and cell cycle progression: Study with synchronized cultures of green alga *Chlamydomonas reinhardtii*. *Journal of Plant Physiology*, 208, 84–93. <https://doi.org/10.1016/j.jplph.2016.10.008>
- Qu, J., Xu, S., Zhang, Z., Chen, G., Zhong, Y., Liu, L., Zhang, R., Xue, J., & Guo, D. (2018). Evolutionary, structural and expression analysis of core genes involved in starch synthesis. *Scientific Reports*, 8, 12736. <https://doi.org/10.1038/s41598-018-30411-y>
- Ral, J. P., Colleoni, C., Wattedled, F., Dauvillée, D., Nempont, C., Deschamps, P., Li, Z., Morell, M. K., Chibbar, R., Purton, S., d'Hulst, C., & Ball, S. G. (2006). Circadian clock regulation of starch metabolism establishes GBSS1 as a major contributor to amylopectin synthesis in *Chlamydomonas reinhardtii*. *Plant Physiology*, 142, 305–317. <https://doi.org/10.1104/pp.106.081885>
- Rammesmayr, G., & Praznik, W. (1992). Fast and sensitive simultaneous staining method of Q-enzyme, α -amylase, R-enzyme, phosphorylase and soluble starch synthase separated by starch-polyacrylamide gel electrophoresis. *Journal of Chromatography A*, 623, 399–402. [https://doi.org/10.1016/0021-9673\(92\)80384-7](https://doi.org/10.1016/0021-9673(92)80384-7)
- Raynaud, S., Ragel, P., Rojas, T., & Mérida, A. (2016). The N-terminal part of *Arabidopsis thaliana* starch synthase 4 determines the localization and activity of the enzyme. *The Journal of Biological Chemistry*, 291, 10759–10771. <https://doi.org/10.1074/jbc.M115.698332>
- Rehmann, H., Wittinghofer, A., & Bos, J. L. (2007). Capturing cyclic nucleotides in action: Snapshots from crystallographic studies. *Nature Reviews. Molecular Cell Biology*, 8, 63–73. <https://doi.org/10.1038/nrm2082>
- Robert, X., Haser, R., Gottschalk, T. E., Ratajczak, F., Driguez, H., Svensson, B., & Aghajari, N. (2003). The structure of barley α -amylase isozyme 1 reveals a novel role of domain C in substrate recognition and binding: A pair of sugar tongs. *Structure*, 11, 973–984. [https://doi.org/10.1016/s0969-2126\(03\)00151-5](https://doi.org/10.1016/s0969-2126(03)00151-5)
- Santelia, D., Trost, P., & Sparla, F. (2015). New insights into redox control of starch degradation. *Current Opinion in Plant Biology*, 25, 1–9. <https://doi.org/10.1016/j.cpb.2015.04.003>
- Scholten, A., Poh, M. K., van Veen, T. A., van Breukelen, B., Vos, M. A., & Heck, A. J. (2006). Analysis of the cGMP/cAMP interactome using a chemical proteomics approach in mammalian heart tissue validates sphingosine kinase type 1-interacting protein as a genuine and highly abundant AKAP. *Journal of Proteome Research*, 5, 1435–1447. <https://doi.org/10.1021/pr0600529>
- Scholten, A., van Veen, T. A., Vos, M. A., & Heck, A. J. (2007). Diversity of cAMP-dependent protein kinase isoforms and their anchoring proteins in mouse ventricular tissue. *Journal of Proteome Research*, 6, 1705–1717. <https://doi.org/10.1021/pr060601a>
- Schreier, T. B., Umhang, M., Lee, S. K., Lue, W. L., Shen, Z., Silver, D., Graf, A., Müller, A., Eicke, S., Stadler-Waibel, M., Seung, D., Bischof, S., Briggs, S. P., Kötting, O., Moorhead, G. B. G., Chen, J., & Zeeman, S. C. (2019). LIKE SEX4 1 acts as a β -amylase-binding scaffold on starch granules during starch degradation. *Plant Cell*, 31, 2169–2186. <https://doi.org/10.1105/tpc.19.00089>
- Schuller, D. J., Grant, G. A., & Banaszak, L. J. (1995). The allosteric ligand site in the V_{max} -type cooperative enzyme phosphoglycerate dehydrogenase. *Nature Structural Biology*, 2, 69–76. <https://doi.org/10.1038/nsb0195-69>
- Schumacher, M. A., Wörmann, M. E., Henderson, M., Salinas, R., Latoscha, A., Al-Bassam, M. M., Singh, K. S., Barclay, E., Gunka, K., & Tschowri, N. (2022). Allosteric regulation of glycogen breakdown by the second messenger cyclic di-GMP. *Nature Communications*, 13, 5834. <https://doi.org/10.1038/s41467-022-33537-w>
- Schwarte, S., Brust, H., Steup, M., & Tiedemann, R. (2013). Intraspecific sequence variation and differential expression in starch synthase genes of *Arabidopsis thaliana*. *BMC Research Notes*, 6, 84. <https://doi.org/10.1186/1756-0500-6-84>
- Seung, D., Thalmann, M., Sparla, F., Abou Hachem, M., Lee, S. K., Issakidis-Bourguet, E., Svensson, B., Zeeman, S. C., & Santelia, D. (2013). *Arabidopsis thaliana* AMY3 is a unique redox-regulated chloroplastic α -amylase. *The Journal of Biological Chemistry*, 288, 33620–33633. <https://doi.org/10.1074/jbc.M113.514794>
- Shinkawa, H., Kajikawa, M., Nomura, Y., Ogura, M., Sawaragi, Y., Yamano, T., Nakagami, H., Sugiyama, N., Ishihama, Y., Kanesaki, Y., Yoshikawa, H., & Fukuzawa, H. (2019). Algal protein kinase, triacylglycerol accumulation regulator 1, modulates cell viability and gametogenesis in carbon/nitrogen-imbalanced conditions. *Plant & Cell Physiology*, 60, 916–930. <https://doi.org/10.1093/pcp/pcz010>
- Sievers, F., Wilm, A., Dineen, D., Gibson, T. J., Karplus, K., Li, W., Lopez, R., McWilliam, H., Remmert, M., Söding, J., Thompson, J. D., & Higgins, D. G. (2011). Fast, scalable generation of high-quality protein multiple sequence alignments using clustal omega. *Molecular Systems Biology*, 7, 539. <https://doi.org/10.1038/msb.2011.75>
- Skrivan, K., Gurrieri, L., Sparla, F., Trost, P., & Blennow, A. (2018). Redox regulation of starch metabolism. *Frontiers in Plant Science*, 9, 1344. <https://doi.org/10.3389/fpls.2018.01344>
- Smith, S. M., Fulton, D. C., Chia, T., Thorneycroft, D., Chapple, A., Dunstan, H., Hylton, C., Zeeman, S. C., & Smith, A. M. (2004). Diurnal changes in the transcriptome encoding enzymes of starch metabolism provide evidence for both transcriptional and posttranscriptional regulation of starch metabolism in *Arabidopsis* leaves. *Plant Physiology*, 136, 2687–2699. <https://doi.org/10.1104/pp.104.044347>

- Sparla, F., Costa, A., Lo Schiavo, F., Pupillo, P., & Trost, P. (2006). Redox regulation of a novel plastid-targeted β -amylase of Arabidopsis. *Plant Physiology*, 141, 840–850. <https://doi.org/10.1104/pp.106.079186>
- Stitt, M., & Zeeman, S. C. (2012). Starch turnover: Pathways, regulation and role in growth. *Current Opinion in Plant Biology*, 15, 282–292. <https://doi.org/10.1016/j.pbi.2012.03.016>
- Strenkert, D., Schmollinger, S., Gallaher, S. D., Salomé, P. A., Purvine, S. O., Nicora, C. D., Mettler-Altmann, T., Soubeyrand, E., Weber, A. P. M., Lipton, M. S., Basset, G. J., & Merchant, S. S. (2019). Multiomics resolution of molecular events during a day in the life of *Chlamydomonas*. *Proceedings of the National Academy of Sciences of the United States of America*, 116, 2374–2383. <https://doi.org/10.1073/pnas.1815238116>
- Sun, Y. J., Rose, J., Wang, B. C., & Hsiao, C. D. (1998). The structure of glutamine-binding protein complexed with glutamine at 1.94 Å resolution: Comparisons with other amino acid binding proteins. *Journal of Molecular Biology*, 278, 219–229. <https://doi.org/10.1006/jmbi.1998.1675>
- Sung, T. Y., Chung, T. Y., Hsu, C. P., & Hsieh, M. H. (2011). The ACR11 encodes a novel type of chloroplastic ACT domain repeat protein that is coordinately expressed with GLN2 in Arabidopsis. *BMC Plant Biology*, 11, 118. <https://doi.org/10.1186/1471-2229-11-118>
- Tardif, M., Atteia, A., Specht, M., Cogne, G., Rolland, N., Brugière, S., Hippler, M., Ferro, M., Bruley, C., Peltier, G., Vallon, O., & Cournac, L. (2012). PredAlgo: A new subcellular localization prediction tool dedicated to green algae. *Molecular Biology and Evolution*, 29, 3625–3639. <https://doi.org/10.1093/molbev/mss178>
- Terashima, M., Specht, M., Naumann, B., & Hippler, M. (2010). Characterizing the anaerobic response of *Chlamydomonas reinhardtii* by quantitative proteomics. *Molecular & Cellular Proteomics*, 9, 1514–1532. <https://doi.org/10.1074/mcp.M900421-MCP200>
- Tetlow, I. J., & Emes, M. J. (2014). A review of starch-branching enzymes and their role in amylopectin biosynthesis. *IUBMB Life*, 66, 546–558. <https://doi.org/10.1002/iub.1297>
- Tetlow, I. J., Wait, R., Lu, Z., Akkasaeng, R., Bowsher, C. G., Esposito, S., Kosar-Hashemi, B., Morell, M. K., & Emes, M. J. (2004). Protein phosphorylation in amyloplasts regulates starch branching enzyme activity and protein–protein interactions. *Plant Cell*, 16, 694–708. <https://doi.org/10.1105/tpc.017400>
- Thyssen, C., Schlichting, R., & Giersch, C. (2001). The CO₂-concentrating mechanism in the physiological context: Lowering the CO₂ supply diminishes culture growth and economises starch utilisation in *Chlamydomonas reinhardtii*. *Planta*, 213, 629–639. <https://doi.org/10.1007/s004250100534>
- Torresi, F., Rodriguez, F. M., Gomez-Casati, D. F., & Martin, M. (2023). Two phosphoenolpyruvate carboxykinases with differing biochemical properties in *Chlamydomonas reinhardtii*. *FEBS Letters*, 597, 585–597. <https://doi.org/10.1002/1873-3468.14590>
- Tunçay, H., Findinier, J., Duchêne, T., Cogez, V., Cousin, C., Peltier, G., Ball, S. G., & Dauvillée, D. (2013). A forward genetic approach in *Chlamydomonas reinhardtii* as a strategy for exploring starch catabolism. *PLoS ONE*, 8, e74763. <https://doi.org/10.1371/journal.pone.0074763>
- Valerio, C., Costa, A., Marri, L., Issakidis-Bourguet, E., Pupillo, P., Trost, P., & Sparla, F. (2011). Thioredoxin-regulated β -amylase (BAM1) triggers diurnal starch degradation in guard cells, and in mesophyll cells under osmotic stress. *Journal of Experimental Botany*, 62, 545–555. <https://doi.org/10.1093/jxb/erq288>
- Wang, H., Gau, B., Slade, W. O., Juergens, M., Li, P., & Hicks, L. M. (2014). The global phosphoproteome of *Chlamydomonas reinhardtii* reveals complex organellar phosphorylation in the flagella and thylakoid membrane. *Molecular & Cellular Proteomics*, 13, 2337–2353. <https://doi.org/10.1074/mcp.M114.038281>
- Wang, L., Patena, W., Van Baalen, K. A., Xie, Y., Singer, E. R., Gavrilenko, S., Warren-Williams, M., Han, L., Harrigan, H. R., Hartz, L. D., et al. (2023). A chloroplast protein atlas reveals punctate structures and spatial organization of biosynthetic pathways. *Cell*, 186(16), e3414. <https://doi.org/10.1016/j.cell.2023.06.008>
- Wang, Q., Pan, J., & Snell, W. J. (2006). Intraflagellar transport particles participate directly in cilium-generated signaling in *Chlamydomonas*. *Cell*, 125, 549–562. <https://doi.org/10.1016/j.cell.2006.02.044>
- Wattebled, F., Ral, J. P., Dauvillée, D., Myers, A. M., James, M. G., Schlichting, R., Giersch, C., Ball, S. G., & D'Hulst, C. (2003). STA11, a *Chlamydomonas reinhardtii* locus required for normal starch granule biogenesis, encodes disproportionating enzyme. Further evidence for a function of α -1,4 glucanotransferases during starch granule biosynthesis in green algae. *Plant Physiology*, 132, 137–145. <https://doi.org/10.1104/pp.102.016527>
- Xiao, Z., Storms, R., & Tsang, A. (2006). A quantitative starch-iodine method for measuring alpha-amylase and glucoamylase activities. *Analytical Biochemistry*, 351, 146–148. <https://doi.org/10.1016/j.ab.2006.01.036>
- Yu, T. S., Zeeman, S. C., Thorneycroft, D., Fulton, D. C., Dunstan, H., Lue, W. L., Hegemann, B., Tung, S. Y., Umamoto, T., Chapple, A., Tsai, D. L., Wang, S. M., Smith, A. M., Chen, J., & Smith, S. M. (2005). α -Amylase is not required for breakdown of transitory starch in Arabidopsis leaves. *The Journal of Biological Chemistry*, 280, 9773–9779. <https://doi.org/10.1074/jbc.M413638200>
- Zaffagnini, M., Bedhomme, M., Groni, H., Marchand, C. H., Puppo, C., Gontero, B., Cassier-Chauvat, C., Decottignies, P., & Lemaire, S. D. (2012). Glutathionylation in the photosynthetic model organism *Chlamydomonas reinhardtii*: A proteomic survey. *Molecular & Cellular Proteomics*, 11(M111), 014142. <https://doi.org/10.1074/mcp.M111.014142>
- Zeeman, S. C., Kossmann, J., & Smith, A. M. (2010). Starch: Its metabolism, evolution, and biotechnological modification in plants. *Annual Review of Plant Biology*, 61, 209–234. <https://doi.org/10.1146/annurev-arplant-042809-112301>
- Zhan, Y., Marchand, C. H., Maes, A., Mauries, A., Sun, Y., Dhaliwal, J. S., Uniacke, J., Arragain, S., Jiang, H., Gold, N. D., Martin, V. J. J., Lemaire, S. D., & Zerges, W. (2018). Pyrenoid functions revealed by proteomics in *Chlamydomonas reinhardtii*. *PLoS ONE*, 13, e0185039. <https://doi.org/10.1371/journal.pone.0185039>
- Zhang, S., Huang, T., Ilangovan, U., Hinck, A. P., & Fitzpatrick, P. F. (2014). The solution structure of the regulatory domain of tyrosine hydroxylase. *Journal of Molecular Biology*, 426, 1483–1497. <https://doi.org/10.1016/j.jmb.2013.12.015>
- Zhang, Y., Pohlmann, E. L., Serate, J., Conrad, M. C., & Roberts, G. P. (2010). Mutagenesis and functional characterization of the four domains of GlnD, a bifunctional nitrogen sensor protein. *Journal of Bacteriology*, 192, 2711–2721. <https://doi.org/10.1128/JB.01674-09>
- Zheng, L., Baumann, U., & Reymond, J. L. (2004). An efficient one-step site-directed and site-saturation mutagenesis protocol. *Nucleic Acids Research*, 32, e115. <https://doi.org/10.1093/nar/gnh110>

SUPPORTING INFORMATION

Additional supporting information can be found online in the Supporting Information section at the end of this article.

How to cite this article: Scholtysek, L., Poetsch, A., Hofmann, E., & Hemschemeier, A. (2024). The activation of *Chlamydomonas reinhardtii* alpha amylase 2 by glutamine requires its N-terminal aspartate kinase–chorismate mutase–tyrA (ACT) domain. *Plant Direct*, 8(6), e609. <https://doi.org/10.1002/pld3.609>